WIS - 93/22 - Mar. Ph

Classical Diffusion, Anderson Localization, and Spectral Statistics in Billiard Chains

T. Dittrich
Institut für Physik, Universität Augsburg, Memminger Straße 6,
W-8900 Augsburg, Germany

E. Doron† and U. Smilansky
Dept. of Nuclear Physics, The Weizmann Institute of Science,
Rehovot 76100, Israel

PACS. 05.45.+b – Theory and models of chaotic systems.
PACS. 03.65.Sq – Semiclassical theories and applications.
PACS. 71.55.Jv – Localization in disordered structures.

Abstract:

We study spectral properties of quasi-one-dimensional extended systems that show deterministic diffusion on the classical level and Anderson localization in the quantal description. Using semiclassical arguments, we relate universal aspects of the spectral fluctuations to features of the set of classical periodic orbits, expressed in terms of the probability to perform periodic motion, that are likewise universal. This allows to derive an analytical expression for the spectral form factor which reflects the diffusive nature of the corresponding classical dynamics. It defines a novel spectral universality class which covers the transition between GOE statistics in the limit of a small ratio of the system size to the localization length, corresponding to the metallic regime of disordered systems, to Poissonian level fluctuations in the opposite limit. Our semiclassical predictions are illustrated and confirmed by a numerical investigation of aperiodic chains of chaotic billiards.

† Present address: H.H. Wills Physics Laboratory, University of Bristol, Tyndall Avenue, Bristol BS8 1TL, UK.

1 Introduction

The study of the relationship between classically chaotic dynamics and its quantum mechanical implications was initially focussed on bound systems, e.g., compact billiards [1–4] and atoms in strong fields [5–7]. In recent years, it has been extended to the investigation of the continuum states associated with such systems, i.e., to the quantal aspects of irregular scattering [8–12]. Both fields have in common that they deal with potentials whose range is restricted to a compact phase-space volume.

The investigation of the effects of classically irregular behaviour in spatially extended, solid-like quantum systems, on the other hand, is still in its infancy [13–15]. It requires to cope simultaneously with *static and dynamic* disorder, both of which pose difficult problems in themselves. Conceptual differences between bounded and extended systems appear both on the classical and on the quantal level: In extended chaotic systems, nearby classical trajectories separate exponentially with a positive Lyapunov exponent, as in bounded chaotic systems. Yet, phase space is *never* covered ergodically in a finite time. Rather, extended systems approach ergodicity only asymptotically through a diffusion process. Hence, basic notions such as that of mixing due to chaotic motion have to be revised. It should be stressed that on the classical level, the diffusive coverage of an extended system is a universal property that does not depend on details of the dynamics, but rather on the dimensionality of the system. Furthermore, it holds both for periodic and aperiodic (random) potentials. On the quantal level, in contrast, the presence or absence of translational symmetry is of decisive importance: Periodic systems show band spectra and extended states, while disordered systems may display a transition to a discrete spectrum with Anderson-localized eigenstates and a concomitant suppression of conductance.

In the present paper, we discuss the implications of an underlying chaotic dynamics for quasi-one-dimensional extended quantum systems. We show that a new type of spectral fluctuations emerges that reflects the diffusive nature of the corresponding classical dynamics, and is different from the standard ensembles of random-matrix theory [16–19]. Using semiclassical arguments, and in particular, generalizing an idea introduced by Hannay and Ozorio de Almeida [20], and by Berry [21, 22], we show that the spectral properties are related to the way phase space is covered by the classical orbits. Specifically, we emphasize the significance of the overall probability for periodic motion as the quantity through which universal aspects of the classical dynamics determine the quantal spectral correlations.

Our analysis forms a natural extension of our previous study of the spectral properties of the quantum kicked rotor [23]. The kicked rotor also belongs to the class of extended systems which show chaos-induced diffusion in the classical limit, and Anderson localization in the quantal case. Therefore, it has much in common with more realistic problems, even though the analogy is only formal. Another application of the same idea was developed in ref.[24]. There, a cluster of chaotic phase-space domains was considered which are interconnected by narrow channels. The fact that the total system possesses an additional time scale, characterizing the flow between the individual domains in the cluster, affects the corresponding energy-level statistics in a crucial way. Finally, arguments similar to those presented here were used to derive the spectral statistics of disordered solids in the mesoscopic domain [25].

The present paper substantiates the semiclassical arguments that form the basis of

the studies mentioned above, by a detailed numerical investigation of a model designed in analogy to a disordered solid [14]: Its building principle is to connect billiard-like cavities, which may induce classically regular or irregular dynamics, by pieces of waveguide to form a quasi-one-dimensional chain. More specifically, we choose a type of billiard element that corresponds to a quarter section of the Sinai billiard [26], i.e., a square with one corner replaced by a quarter circle, bulging into the cavity. These elements are connected in a *zigzag fashion* by intervening rectangular sections adjacent to the shorter straight sides of the billiards (Fig.2.1a)— hence we call our model the "domino billiard" for short. It allows for a transition from pseudointegrable to chaotic classical dynamics, by increasing the radius of the quarter-circle section of the billiard boundary from zero onwards, and a transition from translational symmetry to asymmetry by choosing the lengths of the intervening waveguide sections as a periodic, quasiperiodic, pseudorandom, or random sequence.

We introduce the geometry of the domino billiard in Section 2 and discuss the classical dynamics in this system, focussing on the way an ensemble spreads along the billiard chain. In Section 3, we first give an overview over transport properties and the structure of the eigenstates of the quantized domino billiard for the various cases mentioned above. The main body of this section is devoted to our central topic, the spectral features of this system and their relationship to the corresponding classical dynamics. We summarize our findings in Section 4 and comment on open questions related to our approach. Technical details of the procedure used to quantize the domino billiard are contained in the Appendix.

2 The Domino Billiard: Classical Dynamics

The geometry of the domino billiard is presented in Fig.2.1a. Here and in all that follows, we shall measure lengths in units of the width w of the connecting sections. The other defining parameters of the domino billiard are the radius ρ of the quarter-circle sections of the boundary, and the sequence a_l, $l = 1, 2, 3, \ldots, L$, of the lengths of the intervening sections, where L is the number of billiard elements (corner plus connector) in the chain.

A single "elbow", i.e., a single corner with infinitely long waveguides attached (Fig. 2.1b), is most adequately described as a scatterer [26]. Incoming (outgoing) trajectories are completely defined by their angles $\theta_{i(f)}$, $-\pi/2 < \theta < \pi/2$, with respect to a normal on the boundary line between scatterer and waveguide, and positions $y_{i(f)}$, $0 \le y < 1$, of the intersections with that line. In addition, the information is required whether the trajectory leaves the scatterer on the same side it entered (reflection), or on the opposite side (transmission). The scattering is then characterized by the deflection functions $\theta_f(\theta_i, y_i)$ and $y_f(\theta_i, y_i)$, and the binary-valued function $s(\theta_i, y_i)$, $s = reflection$ or $transmission$.

If the parameter ρ is not exactly zero, scattering off the elbow fulfills the criteria for classical irregular scattering [12]: fluctuations of the deflection functions occur on all scales, there exists a fractal set of trapped trajectories, and the dwell-time distribution decays exponentially for long times. The case $\rho = 0$, on the other hand, may be called "pseudointegrable scattering", generalizing the term "pseudointegrable" coined for closed

billiards with straight edges and angles rationally related to π [27–29]. In pseudointegrable billiards, phase space has the topology of multi-handled tori, formed by a discrete set of sheets between which a trajectory switches at each reflection off the boundary. Likewise, in the domino billiard with $\rho = 0$, the absolute values $|p_\parallel|$, $|p_\perp|$ of the longitudinal and transverse components of the momentum, respectively, are preserved separately, so that there are four such sheets defined by $p_\parallel = \pm|p_\parallel|$, $p_\perp = \pm|p_\perp|$.

The position on the scale from pseudointegrable ($\rho = 0$) to completely chaotic ($\rho \gg 1$) of the scatterers is the decisive parameter to determine the way an ensemble of classical trajectories spreads along the domino billiard. This process is dominated by three time scales, the ballistic time t_b over which a trajectory keeps the memory of its initial condition, the mean hopping time $\langle t_h \rangle$, i.e., the mean dwell time, spent within a single scatterer (more precisely: the time constant describing the exponential decay of the dwell-time distribution [12]), plus the mean transit time, needed to reach an adjacent scatterer, and the diffusion or Thouless time t_d, which is the time required to cover a finite chain of billiards and will be defined below. In the limit of large ρ, it is justified to assume a complete loss of memory of a trajectory at each scattering event such that $t_b \ll \langle t_h \rangle$, and to account for the hopping-time distribution by its variance only. The spreading along the chain is then adequately described as a random walk along the one-dimensional, discrete chain of billiard elements, where the scattering events are completely characterized by probabilities T for transmission and R for reflection. On large temporal and spatial scales, compared to the mean hopping time $\langle t_h \rangle$ and the mean separation $\langle x_h \rangle$ of the scatterers, a continuous probability distribution $p(x,t)$ may be used, where t and x are measured in units of $\langle t_h \rangle$ and $\langle x_h \rangle$, respectively. Its time evolution follows a diffusion equation

$$\frac{\partial}{\partial t} p(x,t) = \frac{D}{2} \frac{\partial^2}{\partial x^2} p(x,t), \tag{2.1}$$

with a diffusion constant

$$D = \frac{T}{R}. \tag{2.2}$$

For sufficiently small ρ, a single scattering event will not completely destroy the correlations in a trajectory, so that t_b exceeds $\langle t_h \rangle$. The description as a Markov process may still be used, however, if a single billiard element is replaced, as constitutive element of the Markov chain, by a number of adjacent ones, and $\langle t_h \rangle$ is scaled up accordingly. We stress that to derive the diffusion equation (2.1), we did not make any assumption as to the nature—periodic or random—of the length sequence a_l of the intervening sections.

For a chain of infinite extension, eq.(2.1) is solved by

$$p(x,t) = \frac{1}{\sqrt{2\pi D t}} \mathrm{e}^{-\frac{(x-x_0)^2}{2Dt}}, \tag{2.3}$$

with an initial condition $p(x,0) = \delta(x - x_0)$. If the chain has a finite length, say $-L/2 \le x \le L/2$, then eq.(2.3) is valid only for short times. The exact solution has to take account of the finite extension of the available space, i.e., it must obey Neumann boundary conditions at the ends of the chain. It reads

$$p(x,t) = \mathrm{Ga}^{(\mathrm{mod}\,2L)}(x - x_0, Dt) + \mathrm{Ga}^{(\mathrm{mod}\,2L)}(x - (L - x_0), Dt), \tag{2.4}$$

where $\mathrm{Ga}^{(\mathrm{mod}\,p)}(x,\Delta) = (1/p)\sum_{n=-\infty}^{\infty}\exp(-2\pi^2n^2\Delta/p^2)\exp(2\pi inx/p)$ is a normalized periodic Gaussian† with period p and variance Δ. The second Gaussian reflects the restriction of diffusion near the boundaries $x_\pm = \pm L/2$. Eq.(2.4) approaches the free-space solution, eq.(2.3), for times shorter than the characteristic time

$$t_d = \frac{L^2}{\pi D}, \tag{2.5}$$

needed to diffusively cover the length L. This defines the Thouless time [30] mentioned above. Asymptotically for $t \gg t_d$, $p(x,t)$ approaches equidistribution over the chain.

An important quantity is the mean probability to return to a point near the initial position x_0 in space. It is obtained by integrating $p(x,t)$ over a suitably chosen spatial bin around x_0, and averaging with respect to x_0. We choose an interval $x_0-d/2 \le x \le x_0+d/2$ as the underlying bin, narrow enough to allow for the approximation $p(x,t) \approx p(x_0,t)$ within the bin. In the limit $d \to 0$, we obtain from eq.(2.4)

$$\begin{aligned} P_r(t) &= \frac{1}{L}\int_{-L/2}^{L/2} \mathrm{d}x_0\, p(x_0,t) \\ &= \frac{1}{L}\sum_{n=0}^{\infty} \mathrm{e}^{-\frac{n^2\pi^2 D}{2L^2}t}. \end{aligned} \tag{2.6}$$

For the two asymptotic regimes mentioned above, this means

$$P_r(t) = \begin{cases} \frac{1}{\sqrt{2\pi Dt}} + \frac{1}{2L}, & t \ll t_d, \\ \frac{1}{L}, & t \gg t_d. \end{cases} \tag{2.7}$$

For later reference, we also introduce the probability for *periodic motion*. It is different from the probability to return in that it refers to a recurrence in *phase space*, rather than in configuration space. For the domino billiard, the energy shell has two dimensions in excess to the position x along the chain in which the dynamics is diffusive: the angle θ of the momentum and the position y across the billiard. Both of them are bounded, and both are covered ergodically on a very short time scale, the ballistic time t_b mentioned above. Therefore, on time scales $t \gg t_b$, we assume equidistribution in these dimensions, and obtain the probability for periodic motion by dividing $P_r(t)$ by $\omega/L = |\mathrm{d}\Omega/\mathrm{d}E|/L$, the ratio of the full energy-shell volume to the extension of the system in the x-direction,

$$P_{pm}(t) = \frac{1}{\omega}\sum_{n=0}^{\infty} \mathrm{e}^{-\frac{n^2\pi^2 D}{2L^2}t} \to \begin{cases} \frac{L}{\omega}\left(\frac{1}{\sqrt{2\pi Dt}} + \frac{1}{2L}\right), & t \ll t_d, \\ \frac{1}{\omega}, & t \gg t_d. \end{cases} \tag{2.8}$$

The limit of pseudointegrable scattering, $\rho = 0$, is conceptually more involved than the chaotic case discussed above. The principle differences are that,

† It is related to the Jacobi Theta function by $\mathrm{Ga}^{(\mathrm{mod}\,p)}(x,\Delta) = \frac{1}{p}\vartheta_4\left[\pi(\frac{x}{p}-1), \exp(-2\pi^2\frac{\Delta}{p^2})\right]$.

(i) the ballistic time diverges and the hopping-time distribution is no longer exponential but follows a power law, so that a description in terms of normal diffusion no longer holds, and
(ii) the spreading along the chain now depends very sensitively on the nature of the sequence α_l, specifically, the spreading becomes superdiffusive (ballistic) if this sequence is periodic and subdiffusive if it is random.
A detailed discussion of the pseudointegrable domino billiard is deferred to a separate publication [31].

Fig.2.2 gives a synopsis of the classical spreading, in terms of the time evolution of $P_r(s)$ of an initially localized ensemble, for the various cases discussed above. Here, we use a single billiard element as the bin underlying the definition of this quantity, and path length s, instead of time, as its argument. In order to generate periodic as well as pseudorandom chains from a single deterministic equation, the sequence α_l of the connector lengths has been determined according to

$$\alpha_l = \beta\rho\left[1 + \left(\mu(l+l_0)^2\right) \bmod 1\right]. \tag{2.9}$$

This rule is motivated by an analogous relation occurring naturally in the case of the quantum kicked rotor (see, e.g., ref.[32]), where the parameter μ is closely related to the relative quantum of action. It generates periodic sequences if μ is rational and pseudorandom sequences if it is irrational (in all that follows, we use $\mu = 0.2$ and $\mu = 0.8(\sqrt{5}-1)$, respectively). In the case of a periodic chain (Fig.2.2a), there is a transition, for increasing ρ, from initially ballistic to diffusive spreading. For the pseudorandom chain (Fig.2.2b), the corresponding transition leads from subdiffusive ($P_r(s) \propto s^{-\nu}$, $\nu \approx 1/6$) to diffusive spreading. In both cases, if ρ is finite, the non-diffusive behaviour is transient, and after a characteristic time which decreases with increasing ρ, it gives way to normal diffusion.

3 The Quantum Domino Billiard

The quantization of the domino billiard proceeds naturally in two major steps. In order to solve the Schrödinger equation (which in the present case is equivalent to the Helmholtz equation and to the Maxwell equations in two dimensions) for a single element of the domino (scatterer plus connector), we employ techniques developed in the context of microwave transmission [33, 34] and of electronic states in microstructured conductors [35–37]. The transfer-matrix method, a standard tool in the theory of microwave transmission [33, 34] and of transport in disordered solids [38], is then used to concatenate the elements to a chain and to find the eigenfunctions and eigenvalues for the complete billiard. Details of this partially analytical, partially numerical procedure are deferred to the Appendix.

Before going into the discussion of the spectral properties of the domino billiard, we present a choice of numerical results in order to introduce into the phenomenology of this system. As mentioned above, the disorder in the domino billiard is generated by varying the length of the connecting sections only, while the scattering elements are simply repeated. Accordingly, a good deal of the features of the domino billiard is determined

by the transmission properties of these identical scattering elements. In Fig.3.1, we show the wavenumber dependence of the transmission coefficients for a single open channel (as to the terminology of open and closed channels, see the Appendix), for $\rho = 1$ (a) and $\rho = 10$ (b). Besides singularities at the thresholds where new channels open, there are zeros of the transmission coefficient at intermediate wavenumbers. At these wavenumbers, incoming and reflected wave add up to a standing wave, while the transmitted wave decays exponentially.

An important quantity to globally characterize the eigenstates and transport properties of extended systems is the Lyapunov exponent: If the system consists of a quasi-one-dimensional chain of discrete elements, the wavefunction can be constructed from the successive product of transfer matrices that describe the scattering properties of the individual elements,

$$T^{(L)} = \prod_{l=1}^{L} T_l. \tag{3.1}$$

If the T_l are drawn from an ensemble of random matrices, the respective largest eigenvalues $g^{(L)}$ of the successive partial products $T^{(L)}$ grows roughly according to an exponential law [39],

$$g^{(L)} \approx e^{\lambda L}, \tag{3.2}$$

where λ is the Lyapunov exponent characterizing the system. There is numerical evidence [40,41] that eq.(3.2) remains valid if the T_l form a pseudorandom sequence of the type specified in eq.(2.9), with fast decaying pair correlations. Since, under the iterated application of a matrix, all vectors tend to approach the direction of the eigenvector with the largest eigenvalue, λ can approximately be determined from the expression

$$\begin{aligned} \lambda &= \lim_{L\to\infty} \frac{1}{L} \ln g^{(L)} \\ &= \lim_{L\to\infty} \frac{1}{L} \ln \sqrt{\left|T^{(L)}\psi^{(0)}\right|^2}, \end{aligned} \tag{3.3}$$

using a normalized but otherwise arbitrary initial vector $\psi^{(0)}$.

The Lyapunov exponent is proportional to the inverse localization length: If $\lambda = 0$, the system can accomodate extended eigenstates, otherwise the eigenstates are localized. Fig.3.2 shows the function $\lambda(\kappa)$, where $\kappa = kw/\pi$, both for a periodic and for a pseudorandom chain, and both for pseudointegrable ($\rho = 0$) and for chaotic scatterers (here, $\rho = 1$): In the periodic case, there are continuous bands with $\lambda = 0$, interspersed with gaps where $\lambda > 0$. For the pseudorandom chain, λ is positive everywhere. This result is independent of the type of the scatterers, provided they couple right- and leftgoing waves, or even different channels. It indicates that eigenstates are extended for the periodic chain and localized for the pseudorandom one, while the influence of the classical dynamics is restricted to finer details of the eigenstates. In particular, this implies that the two features commonly associated with one another, classical diffusion and Anderson localization, do not necessarily occur simultaneously in quasi-one-dimensional extended systems: There are systems which exhibit diffusion in the classical limit, but have extended eigenstates—periodic chains of

chaotic subunits—in analogy to the quantum resonances observed in the quantum kicked rotor [32]. Conversely, there exist systems which support localized eigenstates, but show a subdiffusive classical spreading—random chains of pseudointegrable subunits.

A direct inspection of the eigenstates confirms these observations. Fig.3.3 presents two typical eigenstates, for a chain with $L = 100$ elements, in a spatially coarse-grained manner, i.e., for each element l the absolute square of the wavefunction at a specific cross section is plotted. For a periodic chain, the eigenstates take the form of Bloch states in a finite sample (dotted line). For a pseudorandom chain, the eigenstates are exponentially localized (full line).

A quantity immediately related to the localization length is the mean inverse participation ratio,

$$\xi_L^{-1} = \left\langle \sum_{l=1}^{L} |\psi^{(l)}|^4 \right\rangle, \tag{3.4}$$

where the angle brackets indicate an average over an ensemble of realizations of the static disorder, with the energy restricted to some finite interval (this kind of average will be discussed in more detail below). Fig.3.4a shows the probability distribution of ξ_L^{-1} for the pseudorandom chain with $\rho = 10$, $\langle \alpha \rangle = 15$, and $L = 10, 20, 50, 100$, in the wavenumber range $1.10 \leq \kappa \leq 1.15$. For a system with a constant Lyapunov exponent, these distributions should be Gaussian, by analogy to Anderson-localized states in disordered solids [38, 42]. However, as Fig.3.2 demonstrates, λ varies strongly with energy in the case of the domino billiard: The distribution of λ within the energy interval given above is plotted in the inset in Fig.3.4. The fact that this distribution roughly coincides with the various $P(\xi_L^{-1})$ indicates that for a fixed λ, the distribution of the inverse participation ratio must be fairly sharply peaked.

We now turn to the central issue of this paper, the spectral fluctuations characterizing the domino billiard, and their relationship to the corresponding classical dynamics. We concentrate on the fluctuations since they predominantly contain information on the dynamical properties of the system. In contrast, the mean density, in the case of billiards, is essentially determined by simple geometric features such as size and connectivity. Distinguishing between these two aspects, we presuppose that it is possible to unambiguously decompose the spectral density (also referred to as the density of states, DOS),

$$d(E) = \sum_j \delta(E - E_j), \tag{3.5}$$

into an average and a fluctuating part, i.e.,

$$d(E) = \langle d(E) \rangle + \tilde{d}(E). \tag{3.6}$$

If there is a clear separation of scales in the spectrum, $\langle d(E) \rangle$ can be defined by averaging over the short-wavelength fluctuations, thus restricting its energy dependence to the long-wavelength tendencies. The domino billiard offers the opportunity to replace such a running average or low-pass filtering by a true ensemble mean. It is obtained by averaging over statistically equivalent realizations of the static disorder, given by the connector-length sequence a_l. In this way, the spectral fluctuations can be defined without assuming

spectral ergodicity. Moreover, ensemble averaging does not imply any restriction as to the scale of structures left in the spectral mean. In particular, the fact that the scattering sections in the domino billiard are repeated identically and are therefore not involved in the disorder average, leads to fine-scale features in its mean spectral density, as will be seen below.

There are analytical predictions for the mean spectral density of billiards, in form of the Weyl formula and its subsequent refinements [43], which can be compared with the ensemble average. For billiards whose boundary is composed of sections with smoothly varying curvature, joined at a finite number of corners, and is described by Dirichlet boundary conditions throughout, an improved version of the the Brownell formula (eq.(VI.12) in ref.[43]) gives the most accurate estimate for the mean spectral staircase,

$$\langle N(E)\rangle = \int_0^E \mathrm{d}E' \, \langle d(E')\rangle. \tag{3.7}$$

For a billiard with area σ, circumference Λ, M corners with inner angles φ_m, $m = 1, \ldots, M$ (defined such that "no corner" corresponds to $\varphi = \pi$), and a curvature $\kappa(\lambda)$, $0 \le \lambda < \Lambda$, along the circumference, the mean spectral staircase reads

$$\langle N(k)\rangle = \frac{\sigma}{4\pi}k^2 - \frac{\Lambda}{4\pi}k + \frac{1}{24}\sum_{m=1}^{M}\left(\frac{\pi}{\varphi_m} - \frac{\varphi_m}{\pi}\right) + \frac{1}{12\pi}\int_0^{\Lambda}\mathrm{d}\lambda\,\kappa(\lambda) + O(k^{-\eta}\ln k). \tag{3.8}$$

Here, η, $0 < \eta \le 1$, characterizes the error margin. The dispersion relation $E = E(k)$ depends on the specific application. This means, for the domino billiard with L elements and $\rho > 0$,

$$\langle N(\epsilon)\rangle \approx \frac{\pi}{4}\left[(1+\rho)^2 - \frac{\pi}{4}\rho^2 + \langle\alpha\rangle\right] L\epsilon - \frac{1}{2}\left[1 + \left\{1 + \left(1+\frac{\pi}{4}\right)\rho + \langle\alpha\rangle\right\} L\right]\sqrt{\epsilon} + \frac{L}{48} + \frac{1}{4}. \tag{3.9}$$

Here, $\langle\alpha\rangle$ is the ensemble average of the connector lengths, and $\epsilon = (kw/\pi)^2$ denotes energy in units appropriate to the domino billiard (see eq.(A.4) in the Appendix).

In Fig.3.5, we compare numerical data for the mean spectral staircase with the predictions by eq.(3.9), for the pseudorandom domino billiard with $L = 10$ and one open channel ($1 \le \epsilon < 4$), in the cases $\rho = 1$, $\langle\alpha\rangle = 1.5$ (a) and $\rho = 10$, $\langle\alpha\rangle = 15$ (b). The trend of the spectral staircase is in satisfactory agreement with the refined Weyl formula. Due to the fact that the scattering sections of the domino are not varied but form a periodic element in the chains, an additional structure appears superposed on the predicted smooth increase of $\langle N(\epsilon)\rangle$. One of the irregularities occurs at the threshold $\epsilon = 1$ where the first channel opens. In fact, similar structures appear also at the subsequent thresholds, $\epsilon = 4, 9, \ldots$ (not shown). It is not clear to what extent these inhomogeneities of $\langle N(\epsilon)\rangle$ represent true physics and to what extent they are due to our neglect of tunneling through closed channels in the quantization procedure (see the Appendix). In addition, there are fluctuations of $\langle N(\epsilon)\rangle$ on even smaller scales. They relate to corresponding fluctuations in the Lyapunov exponent λ (the short-dashed lines in Fig.3.5 give the ϵ-dependence of λ), which, in turn, can be ascribed in part to the wavenumber dependence of the transmission

through the scattering elements, and in part form interference effects due to the periodic repetition of these elements: The occurrence of transmissionless states leads to singularities in $\lambda(\epsilon)$ and $\langle d(\epsilon)\rangle$ and thus to steps in $\langle N(\epsilon)\rangle$. Furthermore, it is clear that in the case of a perfectly periodic billiard, the band structure of the spectrum would be reflected in a strong ϵ-dependence of $\langle N(\epsilon)\rangle$. It takes the form of plateaus at the band gaps and a correspondingly steeper increase within the bands, on a scale much smaller than the separation of the channel openings. A similar, if less pronounced, structure persists in the present case. This is illustrated in Fig.3.6, which is analogous to Fig.3.5 but based on data for chains with $\rho = 10$, $\langle\alpha\rangle = 1.5$, in the restricted wavenumber range $1.10 \leq \kappa \leq 1.15$. The plateaus in $\langle N(\epsilon)\rangle$ (full line) are clearly associated with the band gaps of a periodic but otherwise equivalent chain (dotted line).

Throughout this paper, we restrict the spectral statistics to a "sample" $E_c - \Delta E/2 \lesssim E \lesssim E_c + \Delta E/2$ of the spectrum with an extension ΔE small compared to all spectral scales beyond the mean level separation. This is achieved by imposing a weight $\chi(E - E_c)$ such that

$$\chi(E) \approx \begin{cases} 1, & |E| \lesssim \Delta E/2, \\ 0, & \text{else.} \end{cases} \tag{3.10}$$

We also assume that $\chi(E)$ is symmetric around the origin. The truncated spectral density is then defined as

$$d_\chi(E) = d(E)\chi(E - E_c). \tag{3.11}$$

The accumulated density,

$$N_\chi = \int_{-\infty}^{\infty} \mathrm{d}E\, d_\chi(E), \tag{3.12}$$

gives the effective finite dimension of the Hilbert space underlying the truncated spectrum. Specifically, in the following, we shall use the characteristic function of the spectral interval, shifted to the origin,

$$\chi(E) = \Theta\left(\frac{\Delta E}{2} - |E|\right). \tag{3.13}$$

In this case, $N_\chi = \langle d\rangle \Delta E$.

In addition, we "unfold" the spectral density [18, 19], i.e., we use the mean spectral staircase, obtained by averaging numerical spectral data, as a rescaled energy variable,

$$r = \langle N(\epsilon)\rangle, \tag{3.14}$$

so that the spectral density becomes a dimensionless quantity with the average

$$\langle d(r)\rangle \equiv 1. \tag{3.15}$$

Thereby, we assume the transformation (3.14) to be approximately linear within the spectral interval chosen, i.e., $\langle d(E)\rangle = \text{const}$ for $|E - E_c| \lesssim \Delta E/2$, such that the shape of the weight function $\chi(E - E_c)$ is not affected by it (we shall distinguish the transformed from the original functions only by their respective arguments, r or E). For a compound billiard, this implies in particular that the spectral segment must remain within the energy interval between two subsequent channel openings.

We shall restrict our discussion of the spectral fluctuations to the family of statistics that are based on two-point correlations. They contain a good deal of the relevant spectral information and provide a convenient starting point for a semiclassical treatment. The spectral two-point cluster function [16–19] is defined by

$$Y_2(r) = \delta(r) - \left\langle \frac{1}{N_\chi} \int_{-\infty}^{\infty} \mathrm{d}r_0 \tilde{d}_\chi \left(r_0 - \frac{r}{2}\right) \tilde{d}_\chi \left(r_0 + \frac{r}{2}\right) \right\rangle, \tag{3.16}$$

where we have taken into account that $\langle d(r) \rangle \equiv 1$. In this definition, the delta function serves to remove a singularity at $r = 0$ due to self correlations in discrete spectra. By convention [16], the sign has been chosen such that a negative value of the cluster function indicates positive level correlations, and vice versa.

All other two-point spectral statistics can be obtained from the two-point cluster function by one or more integrations. E.g., the number variance, defined as [18, 19]

$$\Sigma^2(r) = \left\langle (N(r) - r)^2 \right\rangle, \tag{3.17}$$

is related to the two-point cluster function by

$$\Sigma^2(r) = r - 2 \int_0^r \mathrm{d}s\, (r - s) Y_2(s). \tag{3.18}$$

The nearest-neighbour level separation $P(s)$, on the other hand, involves also all the higher-order spectral correlations and therefore cannot be derived from $Y_2(r)$.

A quantity in the time domain, equivalent to the two-point cluster function, is the spectral form factor [16, 19],

$$b_2(\tau) = -2 \int_0^\infty \mathrm{d}r\, Y_2(r) \cos 2\pi r \tau, \tag{3.19}$$

where τ is a dimensionless time, related to t by

$$\tau = \frac{t}{t_e}, \quad t_e = 2\pi\hbar\langle d \rangle. \tag{3.20}$$

As in the energy domain, we shall distinguish functions of dimensionless time from their unscaled counterparts only by their arguments.

The spectral form factor can be explicitly related to the quantum dynamics: In terms of the Green function, the spectral density reads

$$\tilde{d}(r) = -\frac{1}{\pi} \mathrm{Im}\, \mathrm{Tr}[\tilde{G}(r)], \tag{3.21}$$

where $\tilde{G}(E) = G(E) - \langle G(E) \rangle$. By inserting eq.(3.21) into the definition for the cluster function, eq.(3.16), and performing the Fourier transformation that leads to the form factor, we obtain

$$b_2(\tau) = -1 + \left\langle \frac{1}{N_\chi} \left| \frac{1}{\pi} \int_{-\infty}^{\infty} \mathrm{d}r\, \mathrm{e}^{-2\pi i r \tau} \mathrm{Tr}[\tilde{G}(r)] \chi(r - r_c) \right|^2 \right\rangle. \tag{3.22}$$

Equivalently, using the identity $G(E) = (i\hbar)^{-1}\int_0^\infty \mathrm{d}t\, e^{iEt/\hbar}U(t)$, the form factor can be expressed in terms of the propagator $U(t) = \exp(-iHt/\hbar)$ as

$$b_2(\tau) = -1 + \left\langle \frac{1}{N_\chi}\left|\int_{-\infty}^{\infty} \mathrm{d}r'\, e^{2\pi i r_c \tau'}\,\mathrm{Tr}[\tilde{U}(\tau')]\hat{\chi}(\tau-\tau')\right|^2\right\rangle, \tag{3.23}$$

where $\mathrm{Tr}[\tilde{U}(\tau)] = \mathrm{Tr}[U(\tau)] - \delta(\tau)$ and $\hat{\chi}(\tau) = \int_{-\infty}^{\infty} \mathrm{d}r\, e^{-2\pi i r\tau}\chi(r)$. In eq.(3.23), the convolution of $\mathrm{Tr}[\tilde{U}(\tau)]$ with the Fourier transform of the spectral weight function endows *the form factor with a finite time uncertainty* $\Delta\tau$. It is related to the spectral range Δr by $\Delta\tau\Delta r = 1$, which expresses the minimum energy-time uncertainty in the present dimensionless units. Writing $\mathrm{Tr}[U(\tau)]$ in terms of the energy eigenstates and splitting the ensuing double sum into its diagonal and its off-diagonal part,

$$\begin{aligned} b_2(\tau) = \frac{1}{N_\chi}\Big[& 2\sum_{\alpha<\beta}\cos\big(2\pi(r_\alpha - r_\beta)\tau\big)\chi(r_\alpha - r_c)\chi(r_\beta - r_c) \\ & - 2\hat{\chi}(\tau)\sum_\alpha \cos\big(2\pi(r_\alpha - r_c)\tau\big) + \big(\hat{\chi}(\tau)\big)^2\Big], \end{aligned} \tag{3.24}$$

we obtain the form factor in the short-time limit, using $\hat{\chi}(0) = N_\chi$, as

$$b_2(\tau) = -1, \quad \tau \ll \frac{1}{N_\chi}, \tag{3.25}$$

while for long times, such that $\hat{\chi}(\tau) \to 0$,

$$b_2(\tau) = \frac{2}{N_\chi}\sum_{\alpha<\beta}\cos\big(2\pi(r_\alpha - r_\beta)\tau\big)\chi(r_\alpha - r_c)\chi(r_\beta - r_c), \quad \tau \gg 1. \tag{3.26}$$

The long-time limit of $b_2(\tau)$ depends on the nature of the spectral fluctuations. If there are no of systematic degeneracies [44], it reads [21–23]

$$b_2(\tau) \to 0, \quad \tau \gg 1. \tag{3.27}$$

Eq.(3.22) mediates between spectral fluctuations and dynamics and thus provides a starting point for the use of semiclassical methods. Formally, the trace of the Green function is given in terms of classical quantities by the Gutzwiller trace formula [45],

$$\mathrm{Tr}[\tilde{G}(E)] = \frac{1}{\hbar}\sum_j A_j(E)\exp\left[i\left(\frac{S_j(E)}{\hbar} + \mu_j\right)\right], \tag{3.28}$$

with amplitudes

$$A_j(E) = \frac{T_j(E)}{\sqrt{\det(M_j(E) - I)}}. \tag{3.29}$$

The sum in eq.(3.28) comprises all classical periodic orbits j with scaled energy r. S_j and μ_j denote action and Maslov phase associated with orbit j, respectively, T_j its period, and M_j the associated stability matrix. Repetitions and negative-time retracings are contained as separate terms in eq.(3.28).

We assume the spectral segment ΔE to be large in terms of the mean level separation, but small, in particular, on classical scales. That is, we require on the one hand that $\Delta E = 2\pi\hbar/\Delta t \gg 1/\langle d\rangle$. For the weight function specified in eq.(3.13), the corresponding time-domain function, $\hat{\chi}(t) = 2\hbar\sin(\Delta E t/2\hbar)/t$, forms a smooth approximation of a delta function with a width $\Delta t \approx 2\pi\hbar/\Delta E$. On the other hand, we presuppose that ΔE is small enough so that within this range, $\mathrm{d}T_j/\mathrm{d}E \ll \hbar/(\Delta E)^2$. For a billiard, the simple relation $T_j = L_j\sqrt{m/2E}$ holds, where L_j is the length of the orbit. In this case, the condition for $\mathrm{d}T_j/\mathrm{d}E$ reads $\Delta E/E \ll \Delta t/T_j$, or equivalently, $\Delta p/p \ll \Delta L/L_j$. In the language of quantum optics, this means that the states preparable within the truncated Hilbert space should be "squeezed states" much narrower in energy (momentum) than in time (space), in the natural units given by the periodic orbits. With this assumption, we expand

$$S_j(E) \approx S_j(E_c) + (E - E_c)T_j(E_c). \tag{3.30}$$

In the same vein, we replace all other energy-dependent quantities in eqs.(3.28), (3.29) by their respective values at $E = E_c$.

These approximations allow us to write the spectral form factor (switching to dimensionless quantities again) as a double sum over periodic orbits [21,22],

$$b_2(\tau) = -1 + \left\langle \frac{1}{N_\chi}\left|\sum_j A_j(r_c)\mathrm{e}^{\mathrm{i}(S_j(r_c)+\mu_j)}\hat{\chi}(\tau-\tau_j)\right|^2\right\rangle. \tag{3.31}$$

In order to push the use of classical information further, it is helpful to split the double sum in eq.(3.31) into its diagonal and off-diagonal parts. This necessitates to be specific about which pairs of orbits should be regarded as identical and which as distinct: It is appropriate not to refer to a full coincidence of the classical phase-space representations of the orbits, but only to the identity of the associated amplitudes and actions. In this way, the simplest type of quantum interference can be taken into account within the diagonal part of the sum, the constructive interference between pairs (or larger sets) of orbits that are related by any discrete symmetry that conserves their amplitudes and actions (the distinction between unitary and antiunitary symmetries, however, which crucially affects the spectral fluctuations [46], is beyond the present semiclassical treatment). Accordingly, we write

$$\begin{aligned} b_2(\tau) = -1 &+ \left\langle \frac{g^2}{N_\chi}\sum_\alpha A_\alpha^2\big(\hat{\chi}(\tau-\tau_\alpha)\big)^2\right\rangle \\ &+ \left\langle \frac{g^2}{N_\chi}\sum_{\alpha\neq\beta} A_\alpha A_\beta\,\mathrm{e}^{\mathrm{i}((S_\alpha+\mu_\alpha)-(S_\beta+\mu_\beta))}\hat{\chi}(\tau-\tau_\alpha)\hat{\chi}(\tau-\tau_\beta)\right\rangle, \end{aligned} \tag{3.32}$$

where g denotes the number of symmetry-related replicas of a given orbit, and the indices α, β count only one representative out of each symmetry-related set.

In eq.(3.32), the diagonal part is directly related to the classical dynamics, in a sense to be explained below, while the off-diagonal part forms a semiclassical account of quantal coherence. Lacking sufficient knowledge on the pair correlations of the actions of the long periodic orbits to evaluate the off-diagonal part (see, however, ref.[47]), we concentrate on the diagonal contribution,

$$b_2^{(d)}(\tau) = -1 + \left\langle g^2 \sum_\alpha \frac{\left(\tau_\alpha(r_c)\right)^2}{|\det(M_\alpha(r_c) - I)|} \delta(\tau - \tau_\alpha(r_c)) \right\rangle, \tag{3.33}$$

where we have inserted the expression (3.29) for the amplitudes and replaced the time-domain weight function $(\hat{\chi}(\tau - \tau_\alpha))^2/N_\chi$ by a delta function. This is justified if the width of $\hat{\chi}(\tau)$ is small, $\Delta\tau \ll 1$, which is equivalent to the requirement $\Delta E = 2\pi\hbar/\Delta t \gg 1/\langle d \rangle$ introduced above.

It is possible, however, only within a finite time regime to restrict the semiclassical form factor to its diagonal part, neglecting the quantal interference contained in the off-diagonal terms. This time window corresponds, by the energy-time uncertainty relation, to an interval of energy scales, bounded from below as well as from above by basic scales contained in the spectral segment to which $b_2(\tau)$ refers: If a spectrum shows level repulsion, as is the case for compact chaotic systems, these energy scales are given, respectively, by the mean level separation (1 in the present units) and the overall length of the spectral segment (Δr in these units). For $\tau \ll 1/\Delta r$, irrespective of the nature of the spectrum, $b_2(\tau) \to -1$ (see eq.(3.25)). The lower energy scale defines a break time $\tau^* \approx 1$ beyond which overall destructive interference dominates in the double sum, eq.(3.26), and the form factor, upon averaging over the disorder or over some energy interval, decays to zero [21–23]. Generally, the time τ^* can be interpreted as the ratio of the maximum number of eigenstates coupled by the dynamics (the effective Hilbert-space dimension), to the total Hilbert-space dimension. There is ample numerical and some analytical evidence (see, e.g., ref.[23]) that in extended systems showing Anderson localization, the effective Hilbert-space dimension is determined by the size of a single localization neighbourhood, if the system size L exceeds the localization length ξ. Consequently, the time by which the phase differences in eq.(3.26) approach a random distribution around the unit circle is then given by $\tau \approx \min(1, \xi/L)$. The corresponding energy scale, in turn, is the mean level separation within a subset of states that belong to the same localization neighbourhood.

In addition to these bounds due to quantal coherence, there is a restriction of classical nature to the statistical treatment of dynamical information. It is the spirit of the present approach to relate universal aspects of the spectral relations to features of the classical dynamics that are likewise characteristic of a large class of systems. Such universal features of the classical dynamics are separated from individual properties, either by making use of the self-averaging property of the relevant classical quantities, due to the mixing nature of the chaotic dynamics, or by explicitly averaging over different realizations of some static disorder, where it is present. In both cases, however, it takes some time τ_u until distinct periodic orbits have grown sufficiently dense such that the contributions of individual orbits average out and universal features dominate. A lower bound for τ_u is the period of the shortest periodic orbit [21, 22]. A better estimate is based on the mixing time, which is closely related to the ballistic time t_b mentioned in the previous section. It is proportional

to the inverse Kolmogorov entropy [48] of the classical dynamics. The time uncertainty $\Delta\tau$ implied by the finite extension of the spectral segment is also relevant for τ_{R}, since it determines the temporal separation of the delta functions of finite width comprising the spectral form factor (see eq.(3.32)), below which they begin to coalesce.

It is possible to give an interpretation of the diagonal form factor, eq.(3.33), in terms of a classical quantity, extending the statistical approach on the side of the quantal spectra to the treatment of the periodic orbits on the classical side: The diagonal part forms a sum over squared amplitudes for periodic motion. This suggests that the sum as a whole be related to the overall probability for the classical trajectories to return to their respective starting points in phase space after a given time t. Proceeding as in refs.[20] and [49], we consider a quantity which measures the probability for periodic motion within a given energy shell. It is defined by

$$I_{E_c}(t) = \frac{1}{(2\pi\hbar)^f N_\chi} \int_\Omega \mathrm{d}^{2f} r_0 \, \delta^{(2f-1)}(r_t - r_0) \, \chi(E_c - H(r_0)), \tag{3.34}$$

where Ω denotes the phase-space volume, and $\chi(E)/N_\chi$ is the normalized weight function of width $\Delta E = \Delta r/\langle d \rangle$, as introduced above to define the spectral segment. By $\delta^{(2f-1)}(r_t - r_0)$ we denote a delta function within the invariant manifold to which the classical phase-space flow is restricted [20]. For chaotic systems, this is the $(2f-1)$-dimensional energy shell of size $\omega = |d\Omega/dE|_{E=E_c}$, defined by

$$\delta^{(2f)}(r_t - r_0) = \delta^{(2f-1)}(r_t - r_0) \frac{\delta(H(r_t) - H(r_0))}{\omega}. \tag{3.35}$$

The subscript E_c will be dropped from now on. By the principle of uniformity, introduced by Hannay and Ozorio de Almeida [20],

$$\lim_{T\to\infty} \frac{1}{T} \int_0^T \mathrm{d}t \, I(t) = 1. \tag{3.36}$$

In order to evaluate eq.(3.34), we assume that all periodic orbits are isolated and unstable, which is valid in completely chaotic systems. It is then possible to introduce, individually for each periodic orbit j, coordinates H (energy) and T (traversal time), tangent to the orbit, and a $2(f-1)$-dimensional set $p_\perp$, $q_\perp$ transverse to it [20, 45, 49]. Integration renders the energy weight function in eq.(3.34) a time-selection function $|\mathrm{d}E/\mathrm{d}t|\chi(E_c - E_j(t))/N_\chi$, where the relation $E_j(t)$ is assumed to be unique and invertible, for a specific periodic orbit j, within the given energy interval around E_c. Since the time-selection function has a small relative width, $\Delta T/T_j(E_c) \approx \Delta E/E_c$ (see above), we can replace it by a delta function. For the transverse coordinates $p_\perp$, $q_\perp$, the condition of periodicity results in the Jacobian $\det(M_j - I)$ of the function $r_{\perp t}(r_{\perp 0}) - r_{\perp 0}$, $r_\perp = (p_\perp, q_\perp)$. If we collect, as in the semiclassical calculation, sets of periodic orbits related by a discrete symmetry into single terms with a multiplicity g, we obtain

$$I(t) = g \sum_\alpha \frac{T_\alpha^{(p)}(E_c)}{|\det(M_\alpha(E_c) - I)|} \, \delta(t - T_\alpha(E_c)). \tag{3.37}$$

Again, the time factor $T_\alpha^{(p)}$ denotes the period of the underlying *primitive* orbit, not that of the full one. It gives the magnitude of the set of distinct possible starting points of the periodic orbit, and thus has the character of an additional, continuous degeneracy factor. Comparing eqs.(3.33) and (3.37), we finds that

$$b_2^{(d)}(\tau) = -1 + g\tau I(\tau t_s). \tag{3.38}$$

Here, we have replaced the primitive periods $T_\alpha^{(p)}$ in eq.(3.37) by the full periods T_α as they occur in the corresponding place in eq.(3.33). This approximation is justified by the fact that in a chaotic system, the primitive periodic orbits proliferate exponentially with their period and thus outnumber the compound orbits consisting of repetitions of shorter primitive orbits.

For a general billiard without a magnetic flux, the only symmetry that leads to action-degenerate sets of periodic orbits is time-reversal invariance, so that $g = 2$. In the context of disordered solids, the corresponding enhancement by a factor of 2, with respect to the classical counterpart, of the quantal probability to return is known as "weak localization" [50].

Eq.(3.38) is the central result of our semiclassical analysis. It suggests that the spectral fluctuations in a given universality class, within the intermediate energy and time regimes specified above, are determined by two factors: the symmetry properties characterizing this class, as reflected in the orbit-degeneracy factor g, and the time evolution of the probability for periodic motion, embodied in the function $I(t)$. As a consequence, the existence of distinct universal classical ways of spreading over the accessible phase space, associated with qualitatively different decay modes of $I(t)$ (e.g., different exponents, depending on the dimensionality of the system), should be reflected in correspondingly distinct spectral universality classes. These ideas have been initiated and applied to integrable systems as well as to compact chaotic systems by Berry [21, 22]. We shall now sketch their extension to systems that combine Anderson-localized eigenstates with deterministic diffusion on the classical level.

Strictly speaking, a diffusive classical dynamics is neither a necessary nor a sufficient condition for Anderson localization to occur in quasi-one-dimensional extended systems, as has been mentioned above. Nevertheless, the simultaneous occurrence of both constitutive properties is the generic situation. The classical probability for periodic motion, in the case of diffusion over a quasi-one-dimensional extended system of finite length, has been derived in the previous section. For the sake of transparence, we shall work in the following with the asymptotes,

$$P_{\rm sm}(t) = \begin{cases} \frac{L}{\omega}\left(\frac{1}{\sqrt{2\pi Dt}} + \frac{1}{2L}\right), & t \ll t_d, \\ \frac{1}{\omega}, & t \gg t_d, \end{cases} \tag{3.39}$$

of the exact expression given in eq.(2.8). They are characterized by a crossover from free diffusion to equidistribution over ω, on the Thouless time scale $t_d = L^2/\pi D$. In order to insert eq.(3.39) into the semiclassical expression, eq.(3.38), for the diagonal form factor, it is necessary to convert unscaled time t into the dimensionless time τ employed in spectral

statistics. We use eq.(3.20) and write the mean spectral density (with respect to the scaled energy $\epsilon = (kw/\pi)^2$) approximately as $\langle d \rangle \approx \langle \Delta N(\epsilon) \rangle / \Delta\epsilon = L\langle \Delta n(\epsilon) \rangle / \Delta\epsilon$, where $\langle n(\epsilon) \rangle$ is the mean spectral staircase for a phase-space bin of size ω/L, and $\Delta\epsilon$ is the energy interval, chosen sufficiently small to allow for a linearization of $\langle n(\epsilon) \rangle$. This yields

$$t_s = \frac{4L}{\pi\hbar} \frac{\langle \Delta n \rangle}{\Delta\epsilon}. \tag{3.40}$$

In this way, the two asymptotes of $I(t)$ are obtained as

$$I(\tau t_s) = \frac{P_{pm}(\tau t_s)}{\lim_{\Theta\to\infty} \Theta^{-1} \int_0^\Theta \mathrm{d}\tau' P_{pm}(\tau' t_s)} = \begin{cases} \sqrt{\frac{\hbar L}{8D(\langle \Delta n \rangle / \Delta\epsilon)\tau}} + \frac{1}{2}, & \tau \ll \tau_d, \\ 1, & \tau \gg \tau_d, \end{cases} \tag{3.41}$$

with a crossover time

$$\tau_d = \frac{\hbar L}{4D(\langle \Delta n \rangle / \Delta\epsilon)}. \tag{3.42}$$

Since the scaled Thouless time τ_d and the quantum-mechanical break time $\tau^* = \min(1, \xi/L)$ are independent of one another, a competition arises between them that is essential for the spectral universality class. The ratio

$$\gamma = \frac{1}{\tau_d} = \frac{4D(\langle \Delta n \rangle / \Delta\epsilon)}{\hbar L} \approx \frac{\xi}{L}, \tag{3.43}$$

is the central parameter for this universality class [23], where ξ is the participation ratio of the localized eigenstates (for an infinite system, i.e., $\xi = \lim_{L\to\infty} \xi_L$—see eq.(3.4)), which in turn gives their approximate localization length. As eq.(3.43) indicates, γ can also be given a spatial interpretation: It roughly equals the inverse number of localization neighbourhoods the system comprises. This shows that sweeping γ from 0 through the crossover at $\gamma \approx 1$ to large values amounts to going from large systems, i.e., the isolating regime in the context of disordered solids, to small ones, corresponding to the metallic regime in disordered solids. Inserting eq.(3.41) into eq.(3.38) now allows to discuss the behaviour of the spectral form factor in these regimes on semiclassical grounds.

For $\gamma \ll 1$, i.e., $\tau_d \gg 1$, quantum interference lets the off-diagonal terms in eq.(3.32) dominate before the diffusion process feels the finite length of the sample, so that only the first option in eq.(3.41) enters the expression for the form factor,

$$b_2^{(\gamma)}(\tau) = \begin{cases} \sqrt{\frac{2\tau}{\gamma}} + \tau - 1, & \tau \ll \frac{\gamma}{2}, \\ 0, & \tau \gg \frac{\gamma}{2}. \end{cases} \tag{3.44}$$

Here, we have inserted eq.(3.27) for the quantal long-time asymptote (the classically non-generic regime $\tau \lesssim \tau_s$ has been omitted for clarity.) The limiting form of $b_2(\tau)$, for $\gamma \to 0$, is

$$b_2^{(0)}(\tau) = \begin{cases} -1, & \tau = 0, \\ 0, & \tau > 0. \end{cases} \tag{3.45}$$

Eq.(3.45) indicates that the two-point cluster function vanishes, and thus that the spectral fluctuations are correlation-free (Poissonian).

If, on the other hand, $\gamma \gg 1$, i.e., $\tau_d \ll 1$, the classical probability for periodic motion reaches its long-time asymptote within the quantum-mechanically relevant time interval. Accordingly, both options in eq.(3.41) have to be taken into account, and the semiclassical prediction for the spectral form factor reads

$$b_2^{(\gamma)}(\tau) = \begin{cases} \sqrt{\frac{2\tau}{\gamma}} + \tau - 1, & \tau \ll \frac{2}{\gamma}, \\ 2\tau - 1, & \frac{2}{\gamma} \ll \tau \ll \frac{1}{2}, \\ 0, & \tau \gg \frac{1}{2}. \end{cases} \tag{3.46}$$

In the limit $\gamma \to \infty$, the first option in eq.(3.46) no longer applies, and

$$b_2^{(\infty)}(\tau) = \begin{cases} 2\tau - 1, & \tau \ll \frac{1}{2}, \\ 0, & \tau \gg \frac{1}{2}. \end{cases} \tag{3.47}$$

This is Berry's semiclassical approximation [21, 22] for the spectral form factor associated with the GOE (Gaussian Orthogonal Ensemble, see refs.[16–19]). In this way, the crossover from GOE (eq.(3.47)) to Poissonian spectral fluctuations (eq.(3.45)) with increasing system size, well known both in the context of disordered solids [51–53] and that of dynamical localization [54–59], is reproduced by our semiclassical theory.

In the remainder of the present section, we shall discuss numerical results, obtained for the domino billiard, that confirm and illustrate our semiclassical theory.

In order to keep the numerical effort within reasonable limits, all the results presented in the following have been calculated in the wavenumber range $1 \leq kw/\pi \leq 2$, i.e., for a single open channel. The semiclassical limit, on the other hand, amounts to a separation of the wavelength from *all* other length scales in the system. Therefore, that wavenumber range cannot be called "semiclassical" in a strict sense, even if ρ takes values $\gg 1$. In any case, the agreement between semiclassical prediction and numerical data should not deteriorate, at least, if the parameters were pushed further towards the semiclassical regime.

We chose a radius of curvature for the scattering elements of $\rho = 10$, and generated the connector-length sequence according to eq.(2.9), with $\beta = 1$, so that $10 \leq \alpha_l < 20$ and $\langle \alpha \rangle = 15$. In addition, an ensemble with $\beta = 0.1$, i.e., $1 \leq \alpha_l < 2$, $\langle \alpha \rangle = 1.5$, has also been studied. We have investigated billiard chains of length $L = 10, 20, 50$, and 100, respectively, and have performed ensemble averages by varying the constant l_0 in eq.(2.9) in steps of L. In this way, spectral statistical quantities have been evaluated on the basis of data sets comprising about 73000 energy levels each.

The corresponding classical data, serving, in particular, to determine the diffusion constant D, are based on ensembles of 1000 trajectories each in 100 different realizations of the static disorder, eq.(2.9). The initial conditions have been chosen along a common cross section of the billiard, with random position along that line and random initial angle. The time evolution of the probability to return and the variance for this ensemble have been

calculated using whole billiard elements as bins, i.e., with the index l as a coarse-grained position variable (see Fig.2.3), whence the diffusion constant was determined.

The mean spectral staircase $\langle \Delta n \rangle / \Delta\epsilon$, which also enters the parameter γ, eq.(3.43), was extracted from the spectral data (not from a Weyl-type formula). In this way, the appropriate values of γ for each L could be determined from independent classical and quantal data, without fitting. The results, for the spectral ensembles discussed in the following, are collected in Tables 1 and 2.

In Fig.3.7, we show a comparison of the spectral form factor, $b_2(\tau)$, as obtained from the spectral data, with our semiclassical prediction, eqs.(3.44) and (3.46). In order to check the semiclassical description of the short-time behaviour independently from the obviously crude approximation of the long-time asymptotics, we slightly modified our prediction by artificially imposing a crossover to the exact form factor for the GOE ensemble. The GOE form factor is given by Dyson's expression [16, 17, 19]

$$b_2^{(\mathrm{GOE})}(\tau) = \begin{cases} 2\tau - 1 - \tau \ln(2\tau + 1), & \tau \leq 1, \\ 1 - \tau \ln[(2\tau+1)/(2\tau-1)], & \tau \geq 1. \end{cases} \tag{3.48}$$

We achieve a crossover from $b_2^{(\gamma)}(\tau)$ to $b_2^{(GOE)}(\tau)$ by the construction

$$b_2(\tau) = \begin{cases} p(\tau/\gamma)\, b_2^{(\gamma)}(\tau) + [1 - p(\tau/\gamma)]\, b_2^{(\mathrm{GOE})}(\tau/\gamma), & \gamma \leq 1, \\ p(\tau)\, b_2^{(\gamma)}(\tau) + [1 - p(\tau)]\, b_2^{(GOE)}(\tau), & \gamma > 1. \end{cases} \tag{3.49}$$

with $p(\tau) = \tau_0^2/(\tau^2 + \tau_0^2)$, and $\tau_0 = 0.5$. Furthermore, we have performed a smoothing by imposing a cutoff on the corresponding cluster function $Y_2(r)$ for $r \gtrsim L$ (for reasons to be explained below).

The smallest sample size investigated, $L = 10$ with $\gamma \approx 3.2$ (Fig.3.7a), is near the GOE limit. Indeed, the data are well reproduced by eq.(3.48) (dotted line in the figure), while the comparison with the prediction according to eq.(3.49) (dashed) shows that the semiclassical theory is rather crude in this regime. For smaller values of γ, however, the agreement with the semiclassical prediction is satisfactory, while a description on basis of the GOE ensemble is clearly ruled out. In addition, Fig.3.7 shows that the classically determined diffusion constant yields values of the quantal parameter γ which are even quantitatively surprisingly accurate. The same situation is found in the corresponding comparison for the spectral cluster function (Fig.3.8) and the number variance (Fig.3.9) (the semiclassical curves have been derived from the spectral form factor, eq.(3.49), via the inverse of eq.(3.19) and via eq.(3.18), respectively).

In Fig.3.10a, we chose a different presentation of the form factor. Here, the abscissa has been scaled individually for each data set by the corresponding value of γ, and we have shifted the ordinate by 1 to allow for a logarithmic plot. The semiclassical prediction is represented by its form for small γ (the isolating regime), where in the first option in eq.(3.44), the second term can be neglected,

$$b_2^{(\gamma)}(\tau) = \begin{cases} \sqrt{\frac{2\tau}{\gamma}} - 1, & \tau \ll \frac{\gamma}{2}, \\ 0, & \tau \gg \frac{\gamma}{2}. \end{cases} \tag{3.50}$$

This allows to simultaneously demonstrate two essential aspects of the semiclassical theory, namely
(i) the initial $\sqrt{\tau}$ increase, and
(ii) the scaling of $b_2(\tau)$ with γ in the regime $\gamma \ll 1$, confirmed by the fact that the four graphs included converge, with decreasing γ, towards a limiting function that is well reproduced by eq.(3.50).

Fig.3.10b is analogous to Fig.3.10a, with the exception that no smoothing has been applied to the data. The most conspicuous feature appearing here, compared with the smoothed case, are oscillations of the form factor with a constant period that scales with γ, i.e., with the system size L, in the same way as the universal τ-dependence underlying our semiclassical analysis. This observation is confirmed by the shape of the corresponding cluster functions (Fig.3.8, right column): Superposed on the noisy background, there is a marked peak near $r = L$, i.e., far away from the central maximum of $Y_2(r)$ that incorporates the universal component of the spectral statistics (note that a *negative* peak in $Y_2(r)$ indicates *positive* spectral correlations, see eq.(3.16)). The low-pass filtering applied to obtain the data in Fig.3.7 served just to remove this peak.

Characteristic times and energies, respectively, that scale with L in the present units correspond to times and energies that are constant in units defined with respect to a single element of the chain. Specifically, $r = L$ corresponds to the mean level separation for a single billiard element: If this energy difference is inserted for $r_\alpha - r_\beta$ in the quantal expression for the form factor in the time regime $\tau \gg 1/N_\chi$, eq(3.26), an oscillatory contribution with the correct period is reproduced. The amplitude of this contribution grows as $L - 1$, if the number of eigenenergies involved increases with L. This suggests that the oscillations reflect strong resonances of the scattering off single billiard elements, near the energies of eigenstates of the corresponding closed subunits. Their influence is amplified by constructive interference among the contributions from the L elements. In Figs.3.11,12 we present results analogous to those shown in Fig.3.8 (right column) and Fig.10b, respectively, but for billiard chains with connector lengths given by eq.(2.9) with $\beta = 0.1$, so that $\langle\alpha\rangle = 1.5$. In this way, the random component of the chain is reduced in favour of its repetitive, periodic character. Indeed, the oscillations in $b_2(\tau)$ are even more pronounced now, and the corresponding peak in the cluster function is very sharp, with a weight that increases roughly in proportion to L. So it appears that we observe a coherence phenomenon occurring in systems that are almost but not exactly periodic, so that Bloch theory does not yet apply. A quantitative explanation, however, is presently not at hand.

4 Summary

The purpose of the present work was to investigate the spectral fluctuations in quasi-one-dimensional extended systems that combine a diffusive classical dynamics with Anderson localization on the quantal level. We used semiclassical arguments to relate universal spectral features to aspects of the set of periodic orbits that are characteristic of the classical dynamics, and emphasized the role of the probability for periodic motion as the relevant

dynamical quantity that conveys classical information into the spectral fluctuations.

This strategy allowed us to derive an analytical expression for the spectral form factor, a time-domain quantity from which all two-point spectral statistics can be obtained. It is dominated by quantum interference for very short and very long times. On intermediate time scales, however, the form factor is directly related to an analogous classical quantity. In the present context, the time evolution of the form factor in this regime reflects the power-law decay of the probability for periodic motion in a diffusive dynamics. The spectral two-point correlations thus obtained form a one-parameter family, spanned by the ratio γ of the localization length to the system size. It covers the crossover from GOE spectral statistics in the limit $\gamma \ll 1$, to Poissonian level fluctuations for $\gamma \gg 1$. This crossover is analogous to the transition from the metallic to the isolating regime in the context of quasi-one-dimensional disordered solids.

As a testing ground for our semiclassical theory, we devised a quasi-one-dimensional system, the domino billiard, consisting of a chain of identical, irregularly scattering billiards connected by waveguide sections whose lengths form a pseudorandom sequence. A detailed numerical study of this model confirmed that it belongs to the system class addressed. Its spectral two-point correlations are even quantitatively well described by the semiclassical theory.

A few additional insights provided by the investigation of this specific model deserve mentioning: The periodic version of the domino billiard forms an instance of extended systems which classically show chaotic diffusion but support extended eigenstates and have a band spectrum, in analogy to the quantum resonances occurring in the quantum kicked rotor. If the domino billiard deviates only slightly from exact periodicity and the connectors coupling the scattering elements are narrow, the transmission and spectral properties of these near-identical subunits are amplified by interference among their contributions and strongly affect the spectrum of the full chain. E.g., the level separation typical for a single subunit is reflected in a sharp peak in the spectral two-point correlations and a corresponding marked oscillation in the spectral form factor. Furthermore, the transport properties, in the limit of narrow connecting channels, are strongly influenced by transmissionless states embedded in the regime of transmission through the chain. At wavenumbers where there is perfect reflection, bound states are formed between adjacent scattering elements (analogous to impurity levels in solids). In the case of periodic arrays of chaotic scatterers, supporting extended states as mentioned above, the high density of these exceptional wavenumbers may give a hint how ballistic quantal transport, due to the simultaneous presence of extended states, can be reconciled with deterministic diffusion in the classical limit.

Improvements and generalizations of the present work are feasible in various directions: In the derivation of eq.(3.38), which relates the spectral form factor to the classical probability to return and is of decisive importance for our approach, we made the crucial assumption that all periodic orbits are isolated and unstable. In fact, there exists an analogous relation for the opposite extreme—integrable systems—which, however, reads different [20,21]: It does not contain the additional time factor occurring in eq.(3.38), which reflects a degeneracy between equivalent starting points along an unstable periodic orbit, besides the time dependence due to the probability for periodic motion. It is

clear that this discrepancy is due to the different dimensionalities of the classical invariant manifolds in both cases. However, a relation analogous to eq.(3.38) is not available for pseudointegrable systems, nor for generic systems with a phase space that encompasses both integrable and chaotic areas. Another shortcoming is that we are not able to describe the crossover from the time regime where the spectral form factor is dominated by the classical dynamics, to the regime where quantal interference prevails. In order to achieve this, a detailed understanding of the off-diagonal part of the periodic-orbit double sum, eq.(3.32), is required [47].

An extension of our semiclassical theory to two-dimensional systems is straightforward and has been applied to a two-dimensional version of the kicked rotor [25], with encouraging results. An extension to three dimensions, however, is far more demanding: It requires a semiclassical understanding of the Anderson transition from localized to extended states at finite disorder. In fact, even the less subtle transition to extended states for vanishing disorder, in one and two dimensions, has not yet been described in semiclassical terms. E.g., it is not clear how a chaotic classical dynamics is reflected in a quantal band structure (if indeed it is). As long as the spectrum is discrete, the notion of orbit degeneracy provides a means to take interference effects due to repetitive structures in the potential into account within the present approach. Our numerical results for a "near-periodic" billiard (see Figs. 3.11,12) demonstrate that the interference between repeated identical subunits of a compound system can indeed drastically affect the spectrum. However, the semiclassical description of band spectra, or of spectra with a fractal measure as they occur at the borderline between localized and extended states [13], necessitates major conceptual revisions.

Finally, we emphasize that the semiclassical approach is by no means restricted to spectral properties, but forms a promising tool also for the description of transport phenomena [60].

Acknowledgement

We acknowledge financial support by the Minerva Foundation and by the Basic Research Foundation of the Israel Academy of Sciences and Humanities (U.S.).

Appendix

This appendix serves to present the technical details of the solution of the Helmholtz equation for the domino billiard, resulting in a secular equation that defines its eigenenergies. The building principle of the domino billiard suggests to divide this task into two main steps: (i), solving the Helmholtz equation for a single element of the domino (scatterer plus connector), and (ii), concatenating the elements to form a chain and finding eigenfunctions and eigenvalues for the complete billiard. Techniques appropriate to step (i) have been developed in the context of microwave transmission [33, 34] as well as that of electronic states in microstructured conductors [35–37], the transfer-matrix method applicable to step (ii) has been adopted from microwave theory [33, 34] and from the theory of disordered solids [38].

Solutions of the Helmholtz equation for a single scattering element, including the adjacent sections of waveguide, are most easily constructed by partitioning this element into the three regions: left waveguide (I), corner (II), and right waveguide (III) (Fig.A.1), and matching the individual solutions along the borderlines.

The waveguides lead, by their finite width, to a quantization of the transverse wavenumber and to the existence of open and closed channels in the longitudinal direction (Fig.A.2). Allowed values for the transverse wavenumber are

$$k_{\perp n} = n\frac{\pi}{w}, \quad n = 1, 2, 3, \ldots . \tag{A.1}$$

By energy conservation, $k^2 = k_\perp^2 + k_\parallel^2 = \text{const}$, eq.(A.1) implies a quantization also of the longitudinal wavenumber (Fig.A.2),

$$k_{\parallel n}^2 = k^2 - \left(\frac{n\pi}{w}\right)^2 . \tag{A.2}$$

For $n\pi/w \leq k$, $k_{\parallel n}$ is real ("open channels"), while for $n\pi/w > k$, $k_{\parallel n}$ is imaginary ("closed channels"). Open channels carry running waves, closed channels evanescent (exponentially decaying) waves. The number of open channels is

$$N = \left[\frac{kw}{\pi}\right], \tag{A.3}$$

where [ ] denotes the integer part. In the following, we shall use dimensionless wavenumbers and energies, defined by

$$\kappa = \frac{kw}{\pi}, \quad \epsilon = \kappa^2, \tag{A.4}$$

such that

$$\begin{aligned} \kappa_{\perp n}^2 &= n^2, \\ \kappa_{\parallel n}^2 &= \kappa^2 - n^2, \\ N &= [\kappa]. \end{aligned} \tag{A.5}$$

It is understood that for $n > N$, the wavenumbers $\kappa_{\|n}$ are chosen as the *positive* imaginary roots $\kappa_{\|n} = i\sqrt{n^2 - \kappa^2}$.

An important feature to be taken into account in the construction of solutions for one complete element, regions I+II+III, is the reflection symmetry of the billiard with respect to the diagonal $x = y$ (see Fig.A.1). As a consequence, there exist two symmetry classes of solutions,

$$\psi^{\pm}(y,x) = \pm\psi^{\pm}(x,y). \tag{A.6}$$

The wavefunctions in regions I and III can now be expressed as

$$\begin{aligned}
\psi_{\nu}^{I\pm}(x,y) &= \sum_{m=1}^{\infty} \left(A_{\nu,m}^{I\pm} e^{i\pi\kappa_{\|m}(y-1)} + B_{n,m}^{I\pm} e^{-i\pi\kappa_{\|m}(y-1)} \right) \sin(m\pi x), \\
\psi_{\nu}^{III\pm}(x,y) &= \sum_{m=1}^{\infty} \left(A_{\nu,m}^{III\pm} e^{i\pi\kappa_{\|m}(x-1)} + B_{\nu,m}^{III\pm} e^{-i\pi\kappa_{\|m}(x-1)} \right) \sin(m\pi y),
\end{aligned} \tag{A.7}$$

They will have to be matched with some convenient set of basis solutions for region II, to which the index ν refers. If we make the additional assumption that the connecting waveguides are sufficiently long, such that evanescent waves originating at the neighbouring scatterers have decayed completely towards the scatterer at issue, we can set

$$B_{n,m}^{I\pm} = B_{n,m}^{III\pm} = 0, \quad \text{for } m > N. \tag{A.8}$$

This truncation amounts to the neglect of tunneling through closed channels. Clearly, it is at its worst for values of κ immediately below the thresholds where new channels open, because there, the decay length $1/\pi\sqrt{n^2 - \kappa^2}$ of the lowermost closed channel ($n = N+1$) diverges.

Solutions for region II are determined by the condition that they vanish on the outer walls and on the quarter circle (which shrinks to a point for $\rho \to 0$). For $\rho > 0$, they have to be calculated numerically [26].

The final step consists in solving the set of coupled linear equations for the coefficients $A_{\nu,m}^{I\pm}$, $B_{\nu,m}^{I\pm}$, $A_{\nu,m}^{III\pm}$, $B_{\nu,m}^{III\pm}$, implied by the condition that the wavefunctions and their first derivatives match along the borderlines $y = 1$, $0 \le x \le 1$ and $x = 1$, $0 \le y \le 1$. In order to restrict this set to a finite size, both the sum over the A-coefficients and the index ν in eq.(A.7) must be truncated at some finite maximum value $M > N$, chosen according to the required numerical accuracy.

In view of the intended use of the solutions thus constructed, it is appropriate to find linear combinations of them such that for the incoming wave (say, from region I), only a single channel is "on",

$$\begin{aligned}
\psi_n^I(x,y) &= e^{-i\pi\kappa_{\|n}(y-1)}\sin(n\pi x) + \sum_{m=1}^{M} r_{n,m} e^{i\pi\kappa_{\|m}(y-1)}\sin(m\pi x), \\
\psi_n^{III}(x,y) &= \sum_{m=1}^{M} t_{n,m} e^{i\pi\kappa_{\|m}(x-1)}\sin(m\pi y).
\end{aligned} \tag{A.9}$$

The coefficients $r_{n,m}$ and $t_{n,m}$ can then be interpreted as reflection and transmission *amplitudes*, respectively.

If the billiard element is considered as a scattering system, all the information required for a complete description is contained in the two $N \times N$ matrices $r_{n,m}$, $t_{n,m}$, where now also m runs over the open channels only, $1 \leq m \leq N$. This information can be organized in various ways. The standard representation is in the form of the S-matrix, which relates the state of the system *after* the scattering to its state *before* the scattering, i.e., the outgoing to the incoming wave. The notions of reflection and transmission, on the other hand, refer to two distinct *spatial* directions.

In the situation described by eq.(A.9), the incoming wave consists of a monochromatic wave in channel n from the left and no flux from the right, while the outgoing wave comprises the reflected wave towards the left and the transmitted wave to the right. Consequently, the relation

$$\begin{pmatrix} r \\ t \end{pmatrix} = S \begin{pmatrix} I \\ 0 \end{pmatrix} \tag{A.10}$$

must hold, where I denotes the $N \times N$ unit matrix, and S is a $2N \times 2N$ matrix. Due to the spatial symmetry of the scatterer (see Fig.A.1 and eq.(A.6)), left and right are indistinguishable, so that

$$\begin{pmatrix} t \\ r \end{pmatrix} = S \begin{pmatrix} 0 \\ I \end{pmatrix} \tag{A.11}$$

must also hold. Eqs.(A.10,11) together imply

$$S = \begin{pmatrix} r & t \\ t & r \end{pmatrix}. \tag{A.12}$$

In addition, invariance with respect to time reversal requires that

$$\begin{pmatrix} I \\ 0 \end{pmatrix} = S \begin{pmatrix} r^* \\ t^* \end{pmatrix}. \tag{A.13}$$

A consequence of this relation is the conservation of flux, separately for each open channel n,

$$1 = \sum_{m=1}^{N} (|r_{n,m}|^2 + |t_{n,m}|^2), \quad 1 \leq n \leq N. \tag{A.14}$$

It is sometimes useful to explicitly distinguish between symmetric and antisymmetric solutions (see eq.(A.6)) also in the S-matrix. By forming the two corresponding components of eq.(A.10), one has

$$r \pm t = s^{\pm} I = s^{\pm}. \tag{A.15}$$

where s^+, s^- now denote $N \times N$ matrices. This implies the relations

$$r = \frac{1}{2}(s^+ + s^-), \quad t = \frac{1}{2}(s^+ - s^-), \tag{A.16}$$

and, by eq.(A.12),

$$S = \frac{1}{2}\begin{pmatrix} s^+ + s^- & s^+ - s^- \\ s^+ - s^- & s^+ + s^- \end{pmatrix}. \tag{A.17}$$

In order to construct solutions for the full billiard chain, a matrix is required that expresses a spatial rather than a temporal relation, namely the relation of the state on the far right of the scatterer to the state on its far left. In analogy to eqs.(A.10), (A.11), and (A.13), the transfer matrix (not to be confused with the T-matrix occurring in scattering theory) is defined by

$$\begin{pmatrix} t \\ 0 \end{pmatrix} = T\begin{pmatrix} 1 \\ r \end{pmatrix}. \tag{A.18}$$

It obeys the relations

$$\begin{pmatrix} r \\ 1 \end{pmatrix} = T\begin{pmatrix} 0 \\ t \end{pmatrix}, \tag{A.19}$$

expressing spatial symmetry, and

$$\begin{pmatrix} 0 \\ t^* \end{pmatrix} = T\begin{pmatrix} r^* \\ 1 \end{pmatrix}, \tag{A.20}$$

due to time-reversal invariance. Together, eqs.(A.18) – (A.20) imply a general expression for the transfer matrix of a single scatterer,

$$T^{(c)}(\kappa) = \begin{pmatrix} [t^*(\kappa)]^{-1} & r(\kappa)[t(\kappa)]^{-1} \\ r^*(\kappa)[t^*(\kappa)]^{-1} & [t(\kappa)]^{-1} \end{pmatrix}. \tag{A.21}$$

Using eq.(A.16) to express the reflection and transmission matrices for the corner by the elements of the S-matrix gives

$$T^{(c)}(\kappa) = \begin{pmatrix} 2(s^{+*} - s^{-*})^{-1} & (s^+ + s^-)(s^+ - s^-)^{-1} \\ (s^{+*} + s^{-*})(s^{+*} - s^{-*})^{-1} & 2(s^{+*} - s^{-*})^{-1} \end{pmatrix}, \tag{A.22}$$

where we have not indicated the wavenumber dependence on the right-hand side for conciseness of notation.

The full transfer matrix for a single element of a domino billiard consists of three factors, one for the scatterer, one for the adjacent section of waveguide, and one factor that takes account of the zigzag shape of the domino billiard. The transfer matrix associated with a straight section of waveguide of length α_l is a diagonal $2N \times 2N$ matrix of phase factors,

$$T_l^{(w)}(\kappa) = \begin{pmatrix} p_l(\kappa) & 0 \\ 0 & p_l^*(\kappa) \end{pmatrix}, \tag{A.23}$$

where

$$(p_l(\kappa))_{n,m} = \delta_{n,m} e^{i\pi\sqrt{\kappa^2 - n^2}\alpha_l}, \quad 1 \le n, m \le N. \tag{A.24}$$

The third factor, for the zigzag shape, takes the form

$$T^{(z)} = \begin{pmatrix} J & 0 \\ 0 & J \end{pmatrix}, \quad J = \begin{pmatrix} 1 & & & & \\ & -1 & & 0 & \\ & & 1 & & \\ & 0 & & -1 & \\ & & & & \ddots \end{pmatrix}, \tag{A.25}$$

where J denotes an $N \times N$ matrix. It introduces an additional phase $e^{i\pi}$ for even-numbered channels. The transfer matrix for the complete chain, consisting of L elements, is then given by the product

$$T^{(L)}(\kappa) = \prod_{l=1}^{L} T_l(\kappa), \quad T_l(\kappa) = T^{(s)} T_l^{(w)}(\kappa) T^{(c)}(\kappa). \tag{A.26}$$

Eigenstates and eigenvalues of the complete domino billiard are determined by the additional requirement that the billiard chain be closed at both ends, i.e., that the wavefunction vanish along two straight lines that form "caps" on the remaining open sides of the first scatterer and the last waveguide section, respectively. In order to derive an explicit condition that incorporates this requirement, we first state a corollary on the general form of the coefficient vector that describes the wavefunction at each cross section between two adjacent elements of the billiard chain. We follow the convention introduced by eq.(A.10) above, that the first N elements in a state vector correspond to rightgoing waves, the subsequent N elements to leftgoing waves. Then, state vectors generated by a product of transfer matrices of the type given by eq.(A.26), must have the form

$$\psi^{(l)}(\kappa) = T^{(l)}(\kappa)\psi^{(0)} = \begin{pmatrix} a_1(\kappa) \\ a_2(\kappa) \\ \vdots \\ a_N(\kappa) \\ -a_1^*(\kappa) \\ -a_2^*(\kappa) \\ \vdots \\ -a_N^*(\kappa) \end{pmatrix} \tag{A.27}$$

if $\psi^{(0)}$ has this form. The proof, by induction, is a straightforward calculation and will not be given here.

The subspace of all states that satisfy the boundary condition at the "lower end" of the domino billiard, where the wavefunction is given by $\psi^{(0)}$, is constructed as follows: Since each channel n corresponds to a Fourier component of the wavefunction along the straight line closing the billiard, the amplitudes for right- and leftgoing waves have to cancel separately for each channel. Therefore, the subspace defined by this condition is

spanned by the unit vectors

$$\psi_n^{(0)} = \frac{1}{\sqrt{2}} \begin{pmatrix} 0 \\ \vdots \\ 1 \\ \vdots \\ 0 \\ 0 \\ \vdots \\ -1 \\ \vdots \\ 0 \end{pmatrix} \begin{matrix} \\ \\ -n^{\text{th}} \text{ element} \\ \\ \\ \\ \\ -(N+n)^{\text{th}} \text{ element} \\ \\ \\ \end{matrix} , \quad 1 \le n \le N. \tag{A.28}$$

For an arbitrary vector in this subspace, given by $\psi^{(0)} = \sum_{n=1}^{N} c_n \psi_n^{(0)}$, with $\sum_{n=1}^{N} |c_n|^2 = 1$, the state at the "upper end" of the chain reads $\psi^{(L)}(\kappa) = \sum_{n=1}^{N} c_n \psi_n^{(L)}(\kappa)$. By the same argument as above, in order to satisfy the corresponding boundary conditions also for $\psi^{(L)}(\kappa)$, right- and leftgoing waves have to cancel separately for each channel. Using eq.(A.27), this results in

$$\begin{aligned} 0 &= \left(\psi^{(L)}(\kappa)\right)_n + \left(\psi^{(L)}(\kappa)\right)_{N+n} = \left(\sum_{m=1}^{N} c_m \psi_m^{(L)}(\kappa)\right)_n + \left(\sum_{m=1}^{N} c_m \psi_m^{(L)}(\kappa)\right)_{N+n} \\ &= 2 \sum_{m=1}^{N} c_m \mathrm{Im}\left[(T^{(L)}(\kappa))_{n,m}\right], \quad 1 \le n \le N. \end{aligned} \tag{A.29}$$

These equations are simultaneously solvable if and only if

$$\det\left[\mathrm{Im}\left(\prod_{l=1}^{L} T_l(\kappa)\right)\right] = 0, \tag{A.30}$$

which is the secular equation for the domino billiard.

References

1 S.W. McDonald and A.N. Kaufman, Phys. Rev. Lett. **42**, 1189 (1979).

2 G. Casati, F. Valz-Gris, and I. Guarneri, Lett. Nuovo Cimento **28**, 279 (1980).

3 O. Bohigas, M.-J. Giannoni, and C. Schmit, Phys. Rev. Lett. **52**, 1 (1984).

4 E.J. Heller, Phys. Rev. Lett. **53**, 1515 (1984).

5 G. Casati, I. Guarneri, and D.L. Shepelyansky, IEEE J. of Quantum Electronics **24**, 1420 (1988), and refs. therein.

6 R. Blümel and U. Smilansky, Z. Phys. D **6**, 83 (1987).

7 D. Wintgen, Phys. Rev. Lett. **58**, 1589 (1987).

8 M.C. Gutzwiller, Physica **7D**, 341 (1983).

9 P. Gaspard and S.A. Rice, J. Chem. Phys. **90**, 2242 (1989); *ibid.* 2255 (1989).

10 B. Eckhardt and P. Cvitanovic, Phys. Rev. Lett. **63**, 823 (1989).

11 R. Blümel and U. Smilansky, Physica **36D**, 111 (1989); Phys. Rev. Lett. **64**, 241 (1990).

12 U. Smilansky, in *Chaos and Quantum Physics*, edited by M.-J. Giannoni, A. Voros, and J. Zinn-Justin, Les Houches Lectures LII, North-Holland – Elsevier (Amsterdam, 1992), p. 371, and refs. therein.

13 T. Geisel, R. Ketzmerick, and G. Petschel, Phys. Rev. Lett. **66**, 1651 (1991); *ibid.* **67**, 3635 (1991); *ibid.* **69**, 695 (1992).

14 E. Doron, U. Smilansky, and T. Dittrich, Physica **179B**, 1 (1992).

15 A. Szafer and B.L. Al'tshuler, Phys. Rev. Lett. **70**, 587 (1993).

16 F.J. Dyson, J. Math. Phys. **3**, 140 (1962); *ibid.*, 1191.

17 C.E. Porter, *Statistical Theory of Spectral Fluctuations*, Academic Press, (New York, 1965).

18 T.A. Brody, J. Flores, J.B. French, P.A. Mello, A. Pandey, and S.S.M. Wong, Rev. Mod. Phys. **53**, 385 (1981).

19 O. Bohigas, in the volume cited under ref.[12], p. 87.

20 J.H. Hannay and A.M. Ozorio de Almeida, J. Phys. A **17**, 3429 (1984).

21 M.V. Berry, Proc. R. Soc. A **400**, 229 (1985).

22 M.V. Berry, in the volume cited under ref.[12], p. 251.

23 T. Dittrich and U. Smilansky, Nonlinearity **4**, 59 (1991); *ibid.* 85.

24 U. Smilansky, S. Tomsovic, and O. Bohigas, J. Phys. A **25**, 3261 (1992).

25 N. Argaman, Y. Imry, and U. Smilansky, Phys. Rev. B , in press.

26 E. Doron, U. Smilansky, and A. Frenkel, Phys. Rev. Lett. **65**, 3072 (1990); Physica **50D**, 367 (1991).

27 P.J. Richens and M.V. Berry, Physica **2D**, 495 (1981).

28 B. Eckhardt, J. Ford, and F. Vivaldi, Physica **13D**, 339 (1984).

29 W. Bauer and G.J. Bertsch, Phys. Rev. Lett. **65**, 2213 (1990).

30 D.J. Thouless, Phys. Rev. Lett. **39**, 1167 (1977).

31 T. Dittrich, to be published.

32 F.M. Izrailev and D.L. Shepelyansky, Dokl. Akad. Nauk SSSR **249**, 1103 (1979) [Sov. Phys. Dokl. **24**, 996 (1979)]; Teor. Mat. Fiz. **43**, 417 (1980) [Theor. Math. Phys. **43**, 553 (1980)].

33 *Principles of Microwave Circuits* edited by C.G. Montgomery, R.H. Dicke, and E.M. Purcell, Dover (New York, 1947).

34 *Field Theory of Guided Waves* by R.E. Collin (2nd edition), IEEE Press (New York, 1991).

35 R.L. Schult, D.G. Ravenhall, and H.W. Wyld, Phys. Rev. B **39**, 5476 (1989).

36 Y. Avishai and Y.B. Band, Phys. Rev. Lett. **62**, 2527 (1989).

37 J. Martorell, S. Klarsfeld, D.W.L. Sprung, and H. Wu, Sol. Stat. Comm. **78**, 13 (1991).

38 K. Ishii, Prog. Theor. Phys. Suppl. **53**, 77 (1973).

39 H. Furstenberg, Trans. Am. Math. Soc. **108**, 377 (1963).

40 M. Griniasty and S. Fishman, Phys. Rev. Lett. **60**, 1334 (1988).

41 N. Brenner and S. Fishman, Nonlinearity **5**, 211 (1992).

42 P.W. Anderson, D.J. Thouless, E. Abrahams, and D.S. Fisher, Phys. Rev. B **22**, 3519 (1980).

43 *Spectra of Finite Systems* by H.P. Baltes and E.R. Hilf, Bibliographisches Institut (Zürich, 1976).

44 J.P. Keating, Nonlinearity **4**, 309 (1991).

45 M.C. Gutzwiller, J. Math. Phys. **8**, 1979 (1967).

46 R. Blümel and U. Smilansky, Phys. Rev. Lett. **69**, 217 (1992).

47 N. Argaman, E. Doron, J. Keating, A. Kitaev, M. Sieber, and U. Smilansky, preprint WIS-92/73/Sept-PH, Weizmann Institute of Science (Rehovot, 1992).

48 See, e.g., *Deterministic Chaos* by H.G. Schuster (2nd edition), VCH (Weinheim, 1989), pp. 29 – 30.

49 *Hamiltonian Systems: Chaos and Quantization* by A.M. Ozorio de Almeida, Cambridge University Press (Cambridge, 1988), pp. 69 – 73.

50 S. Chakravarty and A. Schmid, Phys. Rep. **140**, 193 (1986).

51 N.F. Mott, Philos. Mag. **22**, 7 (1970).

52 U. Sivan and Y. Imry, Phys. Rev. B **35**, 6074 (1987).

53 B.L. Al'tshuler and B.I. Shklovski, Zh. Eksp. Teor. Fiz. **91**, 220 (1986) [Sov. Phys. JETP **64**, 127 (1986)].

54 M. Feingold, S. Fishman, D.R. Grempel, and R.E. Prange, Phys. Rev. B **31**, 6852 (1985).

55 R. Blümel, J. Goldberg, and U. Smilansky, Z. Phys. D **9**, 95 (1988).

56 F.M. Izrailev, Phys. Rev. Lett. **56**, 541 (1986).

57 F.M. Izrailev, Phys. Lett. A **134**, 13 (1988); J. Phys. A **22**, 865 (1989).

58 F.M. Izrailev, Phys. Rep. **196**, 299 (1990).

59 Y.V. Fyodorov and A.D. Mirlin, Phys. Rev. Lett. **67**, 2049 (1991); *ibid.* 2405.

60 H.U. Baranger, D.P. DiVincenco, R.A. Jalabert, and A.D. Stone, Phys. Rev. B **44**, 10637 (1991).

Table captions

Table 1: Characteristic parameters for the spectral ensembles underlying Figs.3.5 and 3.7–3.10.

Table 2: Characteristic parameters for the spectral ensembles underlying Figs.3.6, 3.11, and 3.12.

Figure captions

Fig.2.1: Geometry of the domino billiard (a) and classical scattering in one of its elements (b).

Fig.2.2: Classical spreading along the domino billiard, in terms of the time evolution of the probability to return, for a periodic chain (a) and a pseudorandom chain (b), both with $\langle\alpha\rangle = 1.5$, and for various values of ρ. The full energy shell for a single billiard element has been used as the phase-space bin defining the probability for periodic motion, and path length s as its argument.

Fig.3.1: Transmission probability for a single domino-billiard element as shown in Fig.2.1b, in the wavenumber range where a single channel is open, for $\rho = 1$ (a) and $\rho = 10$ (b). The dotted lines in (b) indicate the interval from which the spectral data shown in Figs.3.6–3.12 have been collected.

Fig.3.2: Transport along the domino billiard. (a) Lyapunov exponent characterizing the growth of the largest eigenvalue of successive transfer-matrix products along a chain with $\rho = 1$, in the wavenumber range where a single channel is open, for a pseudorandom chain (full line) and a periodic chain (dashed line), both with $\langle\alpha\rangle = 1.5$; (b) as (a), but for $\rho = 10$ and $\langle\alpha\rangle = 15$. The dotted lines in (b) indicate the interval from which the spectral data shown in Figs.3.6–12 have been collected.

Fig.3.3: Typical eigenstates of a domino billiard with 100 elements and $\rho = 1$, $\langle\alpha\rangle = 1.5$, for a pseudorandom chain (full line) and a periodic chain (dashed line).

Fig.3.4: Probability distribution of the inverse participation ratio, ξ_L^{-1}, for $L = 10$, 20, 50, 100, in the wavenumber range $1.10 \leq \kappa \leq 1.15$, for a pseudorandom domino billiard with $\rho = 10$ and $\langle\alpha\rangle = 15$. The inset shows the distribution of the Lyapunov exponent λ for a corresponding infinite chain.

Fig.3.5: Integrated level density for a pseudorandom domino billiard with 10 elements and $\rho = 1$, $\langle\alpha\rangle = 1.5$ (a), $\rho = 10$, $\langle\alpha\rangle = 15$ (b). The dashed lines represent the corresponding results obtained from the refined Weyl formula, eq.(3.9), the short-dashed lines represent the energy dependence of the Lyapunov exponent, in arbitrary units, for an infinite chain of the respective type. The dotted lines in (b) indicate the interval from which the spectral data shown in Figs.3.6–12 have been collected.

Fig.3.6: Integrated level density, in the wavenumber range $1.10 \leq \kappa \leq 1.15$, for a pseudorandom domino billiard with 10 elements and $\rho = 10$, $\langle\alpha\rangle = 1.5$ (full line). The broken lines represent the corresponding energy dependence of the Lyapunov exponent, in arbitrary units, for an infinite chain of the same pseudorandom type (dashed) and a periodic, but otherwise equivalent chain (dotted).

Fig.3.7: Spectral form factor for a pseudorandom domino billiard with $\rho = 10$ and $\langle\alpha\rangle = 15$, for chain lengths $L = 10$ (a), 20 (b), 50 (c), and 100 (d), compared with the semiclassical prediction as given in eq.(3.49) (dashed), and in part (a), with the form factor for the GOE ensemble (dotted). The data have been smoothed by low-pass filtering (see text).

Fig.3.8: Spectral cluster function for a pseudorandom domino billiard with $\rho = 10$ and $\langle\alpha\rangle = 15$, for chain lengths $L = 10$ (a,b), 20 (c,d), 50 (e,f), and 100 (g,h), compared with the semiclassical prediction as derived from eq.(3.49) (dashed).

Fig.3.9: Number variance for a pseudorandom domino billiard with $\rho = 10$ and $\langle\alpha\rangle = 15$, for chain lengths $L = 10$, 20, 50, and 100, compared with the semiclassical prediction as derived from eq.(3.49) (dashed).

Fig.3.10: Spectral form factor for a pseudorandom domino billiard with $\rho = 10$ and $\langle\alpha\rangle = 15$, for chain lengths $L = 10, 20, 50, 100$, compared with the semiclassical prediction for the regime $\gamma \ll 1$, eq.(3.50) (dashed). The dimensionless time argument τ has been rescaled individually for each data set by the corresponding value of γ. In part (a), the data have been smoothed by low-pass filtering (see text), and the function $b_2(\tau) + 1$ is shown to allow for a logarithmic plot.

Fig.3.11: Spectral cluster function for a pseudorandom domino billiard with $\rho = 10$ and $\langle\alpha\rangle = 1.5$, for chain lengths $L = 10$ (a), 20 (b), 50 (c), 100 (d).

Fig.3.12: Spectral form factor for a pseudorandom domino billiard with $\rho = 10$ and $\langle\alpha\rangle = 1.5$, for chain lengths $L = 10, 20, 50, 100$, compared with the semiclassical prediction in the regime $\gamma \ll 1$, eq.(3.50) (dashed). The dimensionless time argument τ has been rescaled individually for each data set by the corresponding value of γ.

Fig.A.1: Partitioning of a single domino-billiard element into regions where different quantization procedures apply. The dotted line indicates the basic spatial symmetry characterizing the S-matrices for this billiard element.

Fig.A.2: Open and closed channels in rectangular waveguides. The quantization of the transverse momentum, $k_\perp$, implies, by energy conservation, a quantization also of the longitudinal momentum, $k_\parallel$. Open channels (full lines) carry running waves, closed channels (dashed lines) carry evanescent waves.

$\rho = 10$, $\langle \alpha \rangle = 15$, $1.10 \leq \kappa \leq 1.15$,
$\Delta\epsilon = 0.1125$, $D = 0.0689$:

L	10	20	50	100
$\langle \Delta N \rangle$	36.49	72.95	182.15	364.05
γ	3.201	1.600	0.6391	0.3193

Table 1

$\rho = 10$, $\langle \alpha \rangle = 1.5$, $1.10 \leq \kappa \leq 1.15$,
$\Delta\epsilon = 0.1125$, $D = 0.101$:

L	10	20	50	100
$\langle \Delta N \rangle$	21.42	42.63	106.16	212.04
γ	2.719	1.353	0.5390	0.2691

Table 2

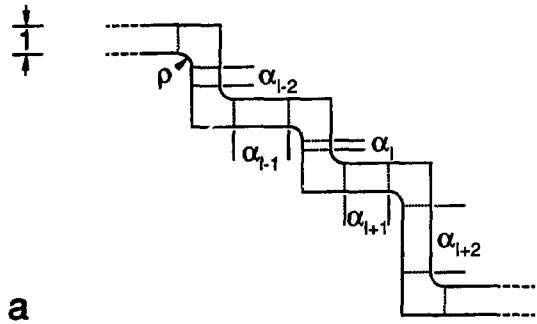
1
ρ
α_{l-2}
α_{l-1}
α_l
α_{l+1}
α_{l+2}

a

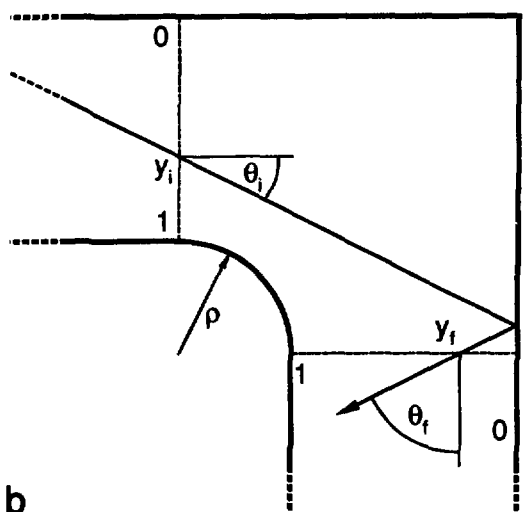
0
y_i
θ_i
1
ρ
y_f
1
θ_f
0

b

FIG. 2.1

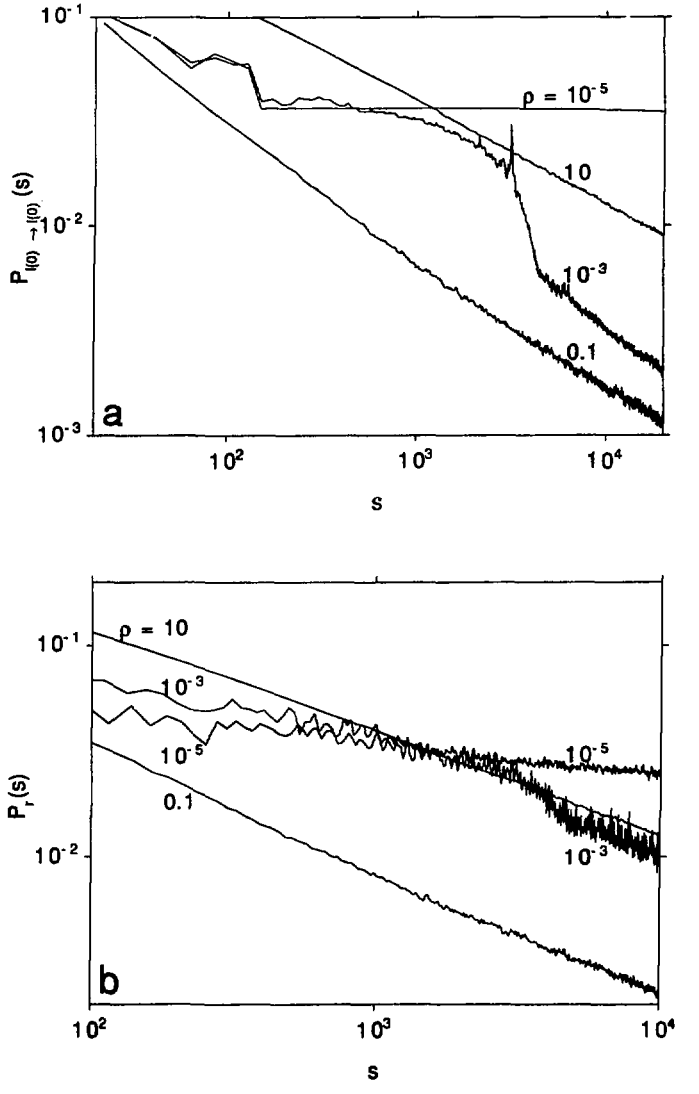
10^{-1}
10^{-2}
10^{-3}
$P_{I(0) \to I(0)}(s)$
$\rho = 10^{-5}$
10
10^{-3}
0.1
a
10^2
10^3
10^4
s
$\rho = 10$
10^{-3}
10^{-5}
0.1
10^{-5}
10^{-3}
$P_r(s)$
b
10^2
10^3
10^4
s

FIG. 2.2

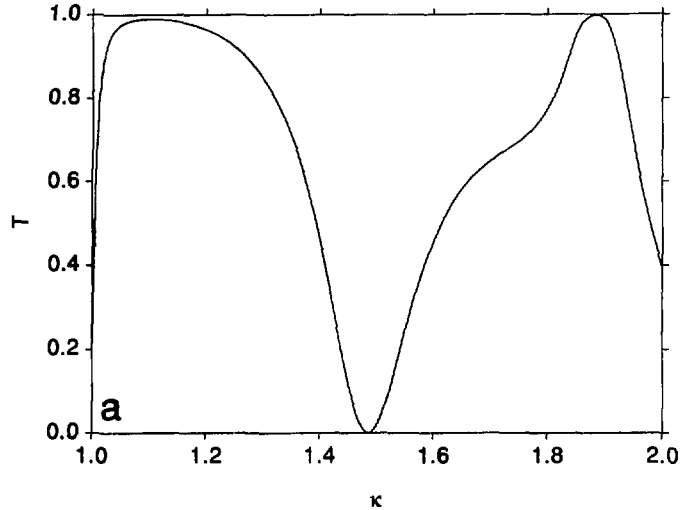
1.0
0.8
0.6
0.4
0.2
0.0
T
a
1.0
1.2
1.4
1.6
1.8
2.0
κ

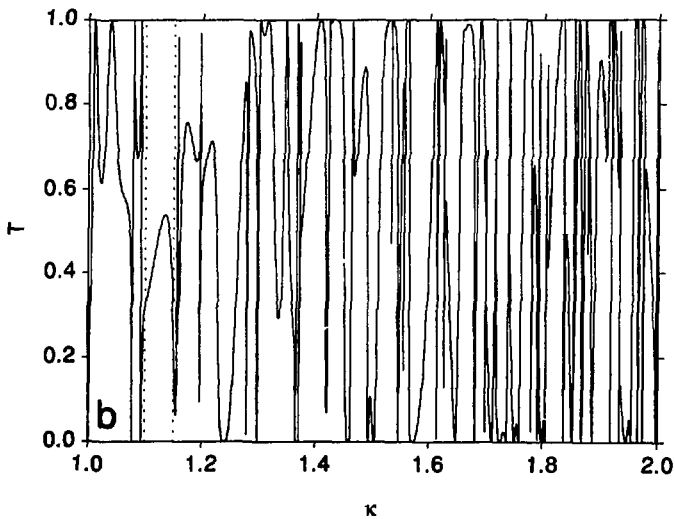
1.0
0.8
0.6
0.4
0.2
0.0
T
b
1.0
1.2
1.4
1.6
1.8
2.0
κ

FIG. 3.1

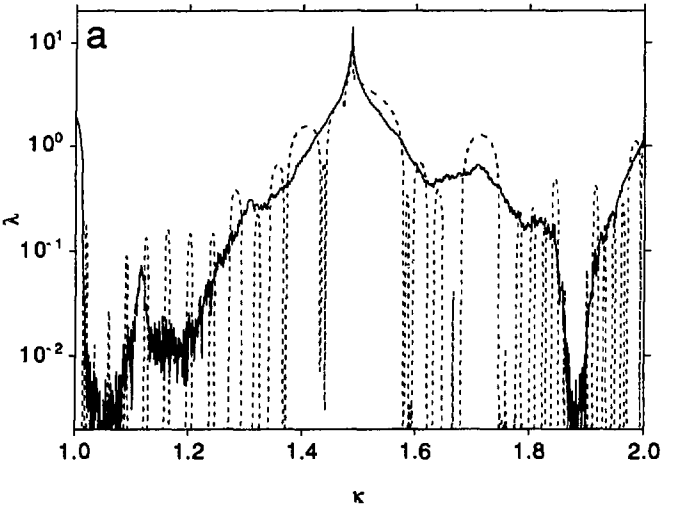
a
10^1
10^0
10^{-1}
10^{-2}
λ
1.0
1.2
1.4
1.6
1.8
2.0
κ

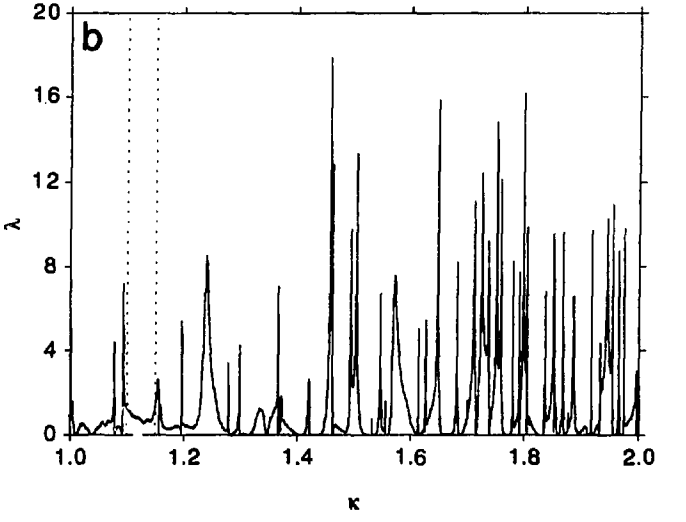
b
20
16
12
8
4
0
λ
1.0
1.2
1.4
1.6
1.8
2.0
κ

FIG. 3.2

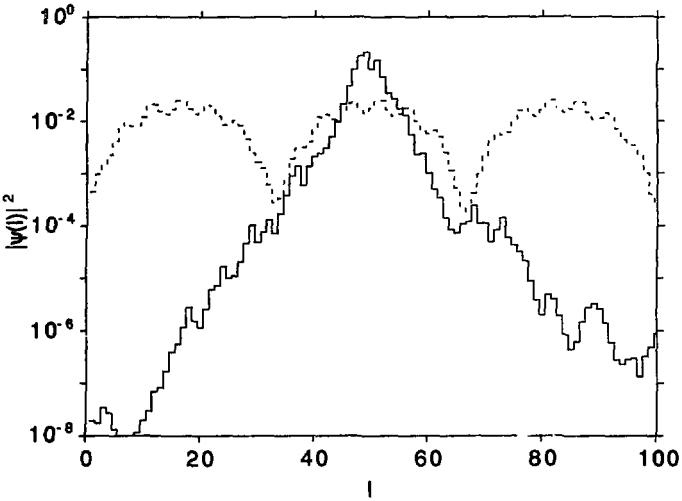

FIG.3.3

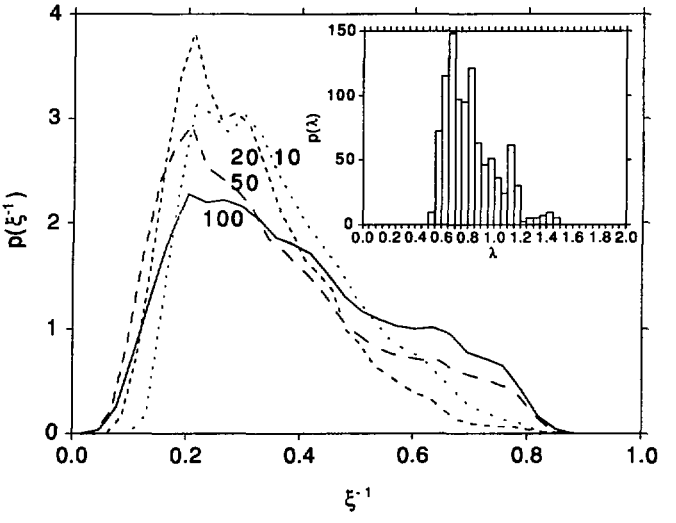
4
3
2
1
0
p(ξ⁻¹)
0.0
0.2
0.4
0.6
0.8
1.0
ξ⁻¹
20
10
50
100
150
100
50
0
p(λ)
0.0 0.2 0.4 0.6 0.8 1.0 1.2 1.4 1.6 1.8 2.0
λ

FIG. 3.9

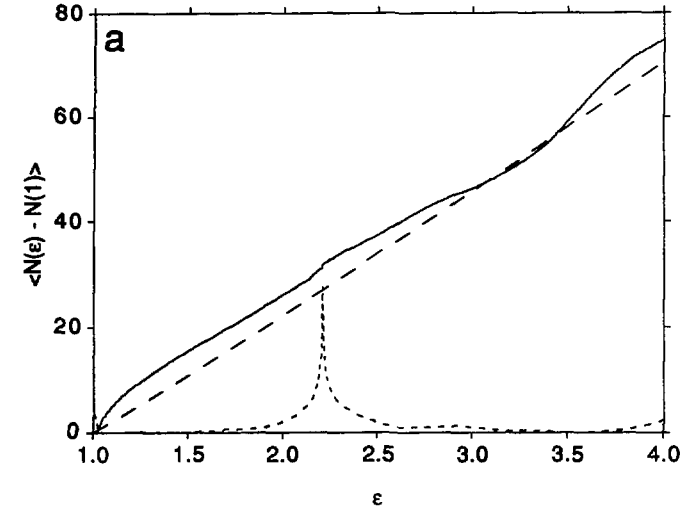
a
80
60
40
20
0
<N(ε) - N(1)>
1.0
1.5
2.0
2.5
3.0
3.5
4.0
ε

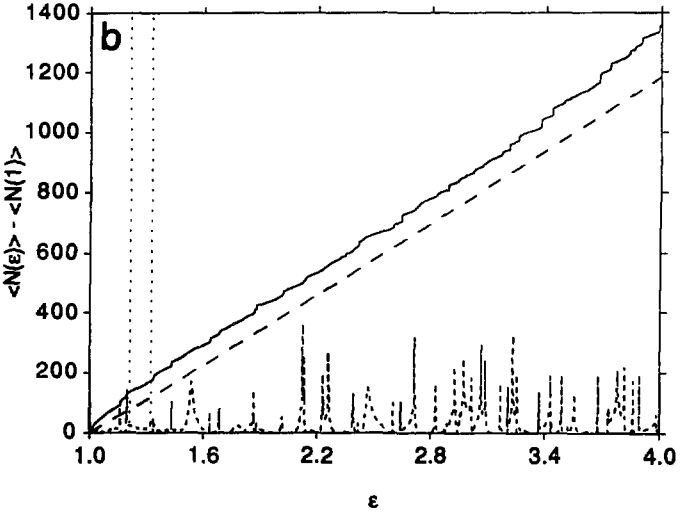
b
1400
1200
1000
800
600
400
200
0
<N(ε)> - <N(1)>
1.0
1.6
2.2
2.8
3.4
4.0
ε

FIG. 3.5

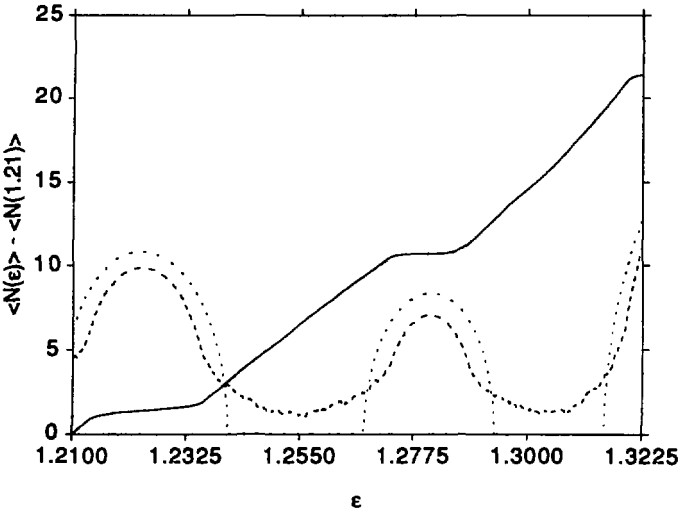

FIG. 3.6

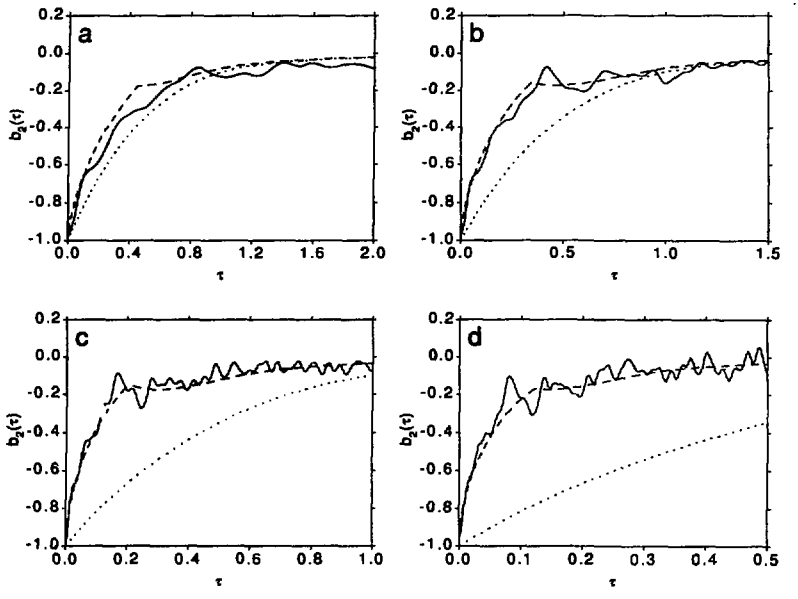
a
b
c
d
$b_2(\tau)$
τ
0.2
0.0
-0.2
-0.4
-0.6
-0.8
-1.0
0.0
0.4
0.8
1.2
1.6
2.0
0.5
1.0
1.5
0.1
0.2
0.3
0.4
0.6

FIG. 3F

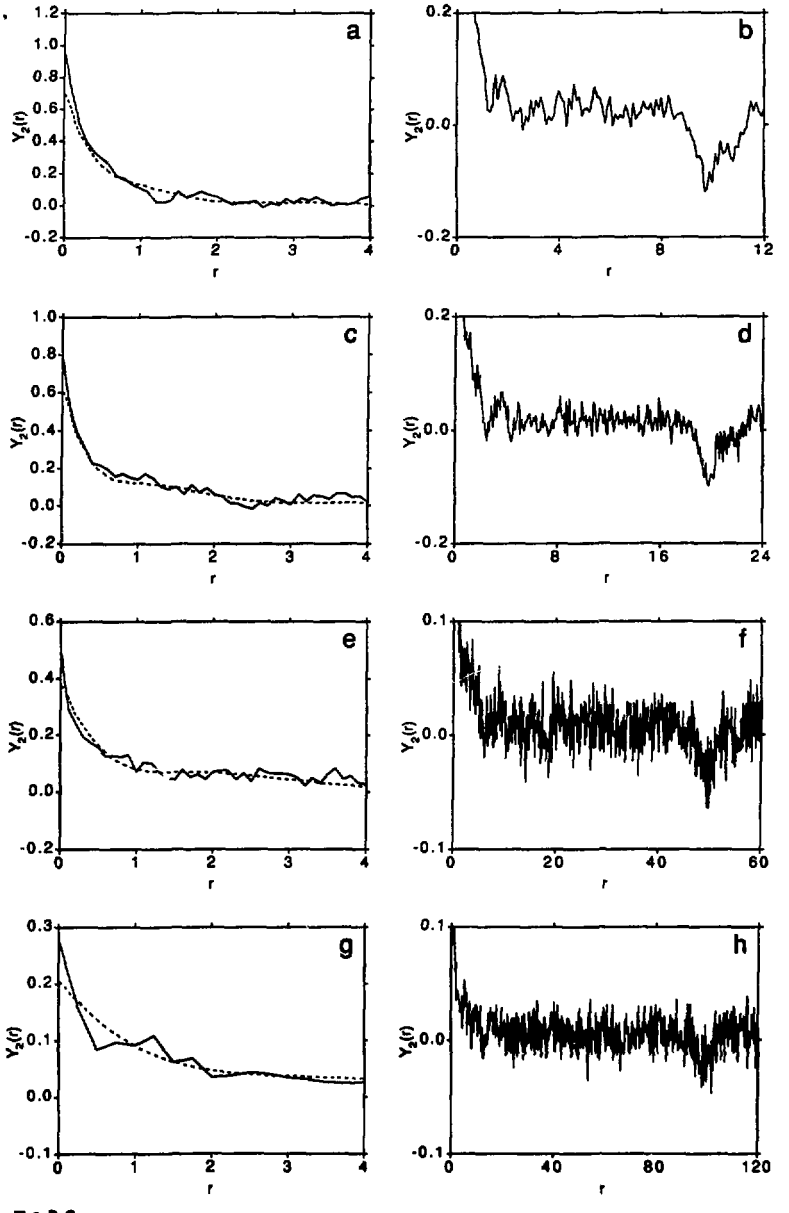

FIG. 3.8

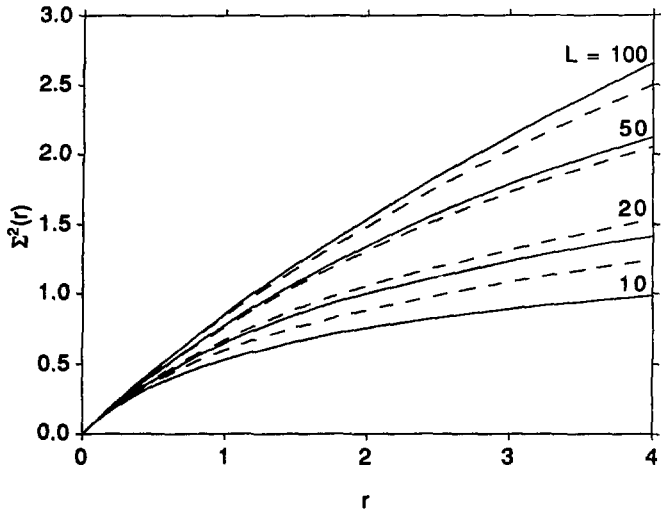

FIG. 3.5

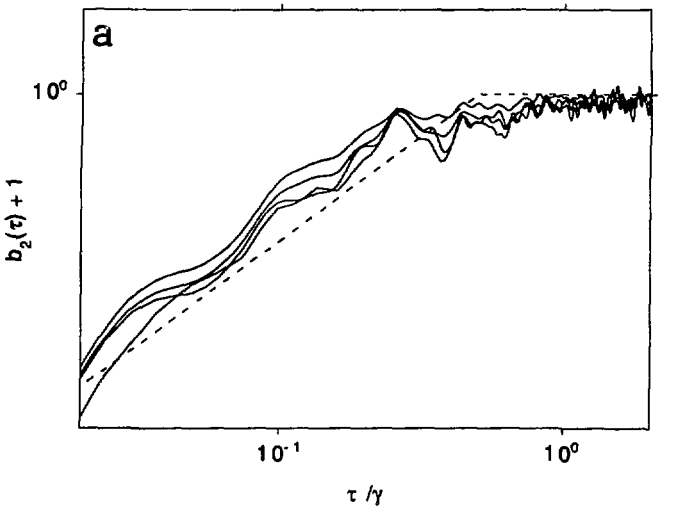
a
10^0
$b_2(\tau) + 1$
10^{-1}
10^0
τ / γ

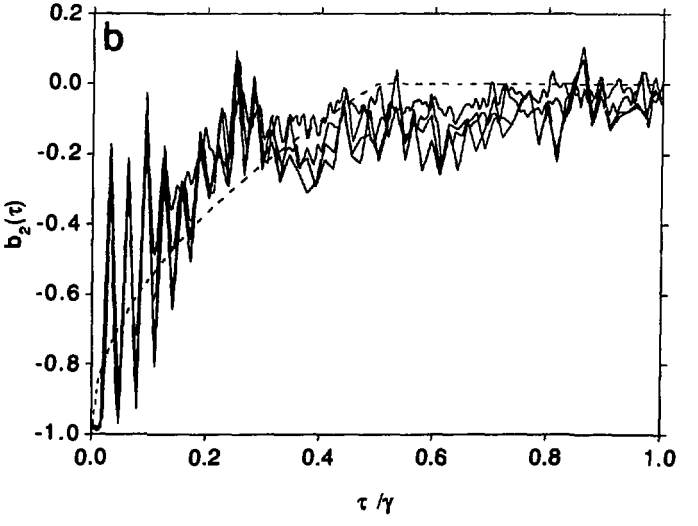
b
0.2
0.0
-0.2
-0.4
-0.6
-0.8
-1.0
$b_2(\tau)$
0.0
0.2
0.4
0.6
0.8
1.0
τ / γ

FIG. 3.10

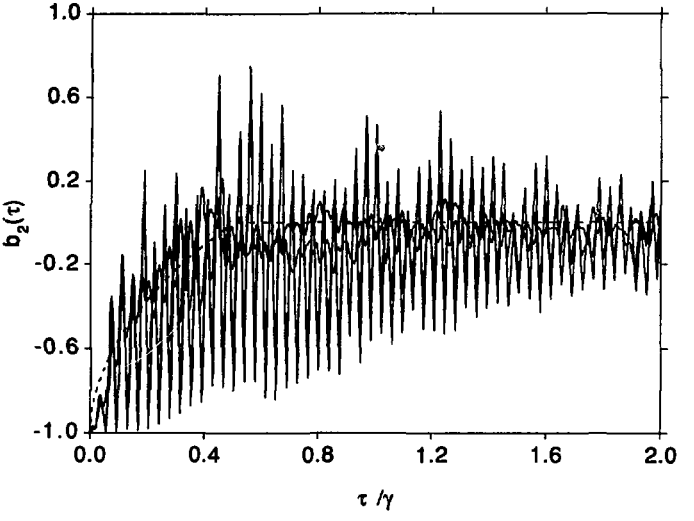

FIG. 3.11

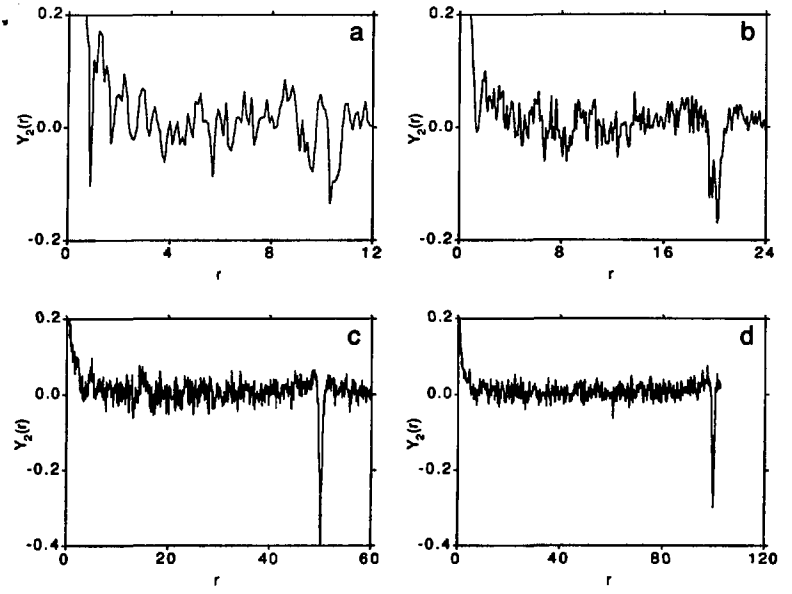

FIG. 3. 12

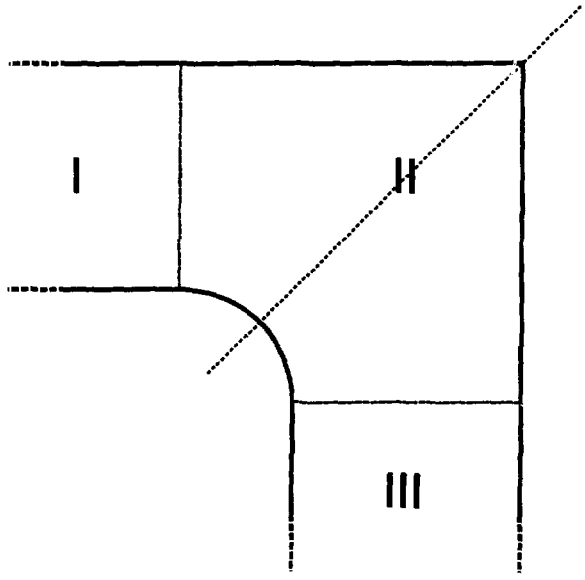

FIG. A.1

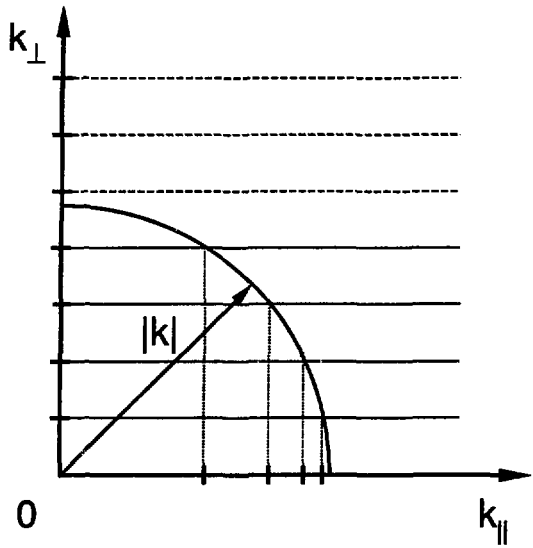

FIG. A.2